



Norwegian University of  
Science and Technology

# The effect of carbon in $\text{MnO}_2$ composite electrodes

**Christian Thesen**

Materials Technology (MIMT)

Submission date: March 2018

Supervisor: Ann Mari Svensson, IMA

Norwegian University of Science and Technology  
Department of Materials Science and Engineering





## Declaration

---

M. Sc Candidate: Christian Thesen

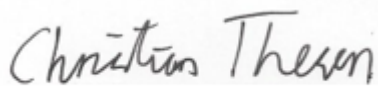
Supervisor: Professor Ann Mari Svennson

Co-supervisor: Ingrid Roten Mattson

This Master's thesis has been conducted at the Department of Materials Science and Engineering, at the Norwegian University of Science and Technology (NTNU). The work for this study has been performed between September 2017 – February 2018.

I hereby declare that the work in this study has been conducted independently, honestly and by the guidelines set by NTNU. All the references used in this thesis has been denoted.

Trondheim, 01.03.2018



Christian Thesen

---

Christian Thesen



## Acknowledgements

---

It goes without saying that writing a Master's thesis and completing a degree is a lot of work. It is not a task you attempt lightly. While the thesis may be a solo venture on paper, it is not in reality. In order to complete a MSc one needs a lot of help from friends, family, co students and supervisors. With that said, I would like to thank everyone that has helped me to get to where I am today.

A special thank you goes to my supervisor Ann Mari Svennson. She has always been available, has given great guidance, motivation and support.

Co supervisor Ingrid Mattson has also been an integral part of the thesis. Her guidance at the lab has been paramount for this work. I also want to thank Magnus Bentzen Følstad, and the rest of the technical staff at kjemi 2. I want to thank Sidsel Meli Hanetho for giving me the recipe to the carbon-based powder used during this thesis. I wish I could mention everyone that helped me, but that list would be quite long. Thus, I want to thank everyone involved, you've been great!



## Abstract:

---

Supercapacitors are promising electrochemical storage devices that might aid in several key technologies such as solar cells, cars, computers and more. In fact, supercapacitors are already used in cars (regenerative braking). They are also used in busses as storage devices that recharge whenever they let on and off passengers. While supercapacitors are considered to be a functioning technology, there are still some challenges that need to be tackled. Most conventional supercapacitors, such as carbon-based capacitors, have a low energy density. Others, such as the well-known metal oxide  $\text{RuO}_2$ , have both a relatively high energy and power density. Unfortunately,  $\text{RuO}_2$  is both expensive and toxic. Better alternatives are needed, and  $\text{MnO}_2$  is a promising substitute. It has a high theoretical capacitance of 1370 F/g, is abundant in the earth's crust, and is harmless. Unfortunately,  $\text{MnO}_2$  suffers from being a messy oxide, forming more crystal structures than the author can count.

The aim of this thesis is to investigate  $\text{MnO}_2$  electrodes with and without carbon added during wet synthesis. The method is based on Ghodbane et al's work. The two electrode variations were either made by adding Ketjenblack during synthesis, or Acetylene Black during electrode processing. In both cases, carbon is added as a conductive additive. The electrode substrate used was Toray paper TGP-H-090, 0.28 mm thick. PTFE was used as a binder. Brunauer-Emmett-Teller (BET) and X-ray diffraction (XRD) was used to investigate the surface area and crystal structure of the materials. Thermogravimetric analysis (TG) was used on the Ketjenblack-based  $\text{MnO}_2$  powder, to measure the carbon content in the powder. The Ketjenblack-based powder had ~25% carbon according to TG. The  $\text{MnO}_2$  electrodes with Acetylene Black only contained ~14% carbon. All powders were tested with electrochemical cycling in a 3-cell setup, with a Biologic VMP 3 potentiostat.

The measured surface areas of the powders used in this thesis were 46  $\text{m}^2/\text{g}$ , 66  $\text{m}^2/\text{g}$ , 408  $\text{m}^2/\text{g}$  for  $\delta\text{-MnO}_2\text{-8-F-2}$ ,  $\delta\text{-MnO}_2\text{-8-3}$ ,  $\delta\text{-MnO}_2\text{-8-F-C}$  respectively. All powders had characteristic Birnessite peaks  $2\theta = 12.2\text{-}12.5$ ,  $24.8\text{-}25$ ,  $37.0\text{-}37.1$ ,  $62.9\text{-}64.6$ . Slight variations in d-values could be attributed to the different variations of synthesis parameters. Notable capacitance values were 501 F/g for the Ketjenblack based electrodes, and 474 F/g for the Acetylene Black based electrodes. Both electrodes were cycled with constant current at 0.1 A/g. The obtained values were measured at the 9<sup>th</sup> and 30<sup>th</sup> cycle respectively. Indicating a 14.4% / 7.7% increase in capacity from the 2<sup>th</sup> cycle. The increase in capacitance indicates that an activation step has occurred in the electrodes. The Ketjenblack based electrodes had the highest capacitance values



overall, which is an indication that adding Ketjenblack during synthesis will improve supercapacitor electrodes. However, too few parallels have been tested, and more research is needed.

## Sammendrag

---

Superkondensatorer er lovende som elektrokjemisk lagringsenheter. De kan være til stor hjelp for teknologier som solceller, biler, datamaskiner m.m. Superkondensatorer er allerede en fungerende teknologi i biler (regenererende bremsing), og i busser som energilagringsenheter som lader på hver busstopp. Selv om superkondensatorer kan sees på som en fungerende teknologi, så er det mange utfordringer som må løses. De fleste konvensjonelle superkondensatorer har lav energitetthet (eksempelvis karbonbaserte superkondensatorer). Det kjente metalloksidet  $\text{RuO}_2$  har derimot oppnådd både høy energi tetthet og strømtetthet. Dessverre er det både dyrt og giftig. Det trengs bedre alternativer, og det er der  $\text{MnO}_2$  kommer på banen. Det har en høy teoretisk kapasitans på 1370 F/g. Det er mye av det i jordskorpen, og det er harmløst. Uheldigvis så er  $\text{MnO}_2$  et «rotete» oksid. Det vil si at er mange forskjellige krystallstrukturer, og det er vanskelig å oppnå ønsket struktur.

Målet med denne rapporten er å se på forskjellen mellom  $\text{MnO}_2$  kompositt elektroder hvor enten Ketjenblack er tilsatt under syntese av pulver, eller hvor Acetylene Black er tilsatt under selve prosesseringen av elektrodene. Oppskriften er basert på Ghodbane et al's arbeid. Karbon blir i begge tilfeller tilsatt for å øke ledningsevnen til elektrodene. Elektrode substratet er karbon Toray papir TGP-H-090, 0.28 mm tykt. PTFE ble benyttet som binder. Brunauer-Emmett-Teller (BET) ble benyttet for å kartlegge overflatearealet til pulverne. Røntgendiffraksjon (XRD) ble benyttet for å utforske krystallstrukturen, og for å identifisere fasene i materialet. Termogravimetrisk analyse (TG) ble benyttet på det Ketjenblack baserte  $\text{MnO}_2$  pulveret. Dette ble gjort for å måle karboninnholdet i pulveret. Her kom det fram at pulveret inneholdt ~25% karbon, mens de andre batchene med pulver fikk tilført ca 14% Acetylene Black under lagging av elektroder. Alle pulverne ble elektrokjemisk syklet i ett 3-celle oppsett, med Biologic VMP 3 potentiostat.

Det målte overflatearealet på pulverne i denne rapporten var på 46  $\text{m}^2/\text{g}$ , 66  $\text{m}^2/\text{g}$ , 408  $\text{m}^2/\text{g}$  for  $\delta\text{-MnO}_2\text{-8-F-2}$ ,  $\delta\text{-MnO}_2\text{-8-3}$ ,  $\delta\text{-MnO}_2\text{-8-F-C}$  respektivt. Alle pulverne hadde karakteristiske Birnessite topper på  $2\theta = 12.2\text{-}12.5$ ,  $24.8\text{-}25$ ,  $37.0\text{-}37.1$ ,  $62.9\text{-}64.6$ . Under sykling ble kapasiteter så høye som 501 F/g oppnådd for prøvene med Ketjenblack.  $\text{MnO}_2$  pulverne med Acetylene Black oppnådde verdier opp imot 474 F/g. I begge tilfeller ble konstant strøm benyttet på 0.1 A/g. Det er også viktig å nevne at de høyeste verdiene fant sted på slutten av hhv. 10/30 sykler, og at det er grunn til å tro at materialet er blitt aktivert. Under elektrokjemisk sykling, er det

mye som tilsier at Ketjenblack tilført under syntese kan være med på å øke kapasiteten til elektroder. Flere paralleller og tester må kjøres for å oppnå en klar konklusjon.



# Table of contents

---

1	Introduction.....	1
2	Theory.....	3
2.1	Capacitance.....	3
2.1.1	Supercapacitance – double layer theory.....	4
2.1.2	Pseudocapacitance.....	5
2.1.3	Electrolytes.....	6
2.2	MnO <sub>2</sub> –Manganese Dioxide.....	7
2.2.1	Properties.....	7
2.2.2	Crystal structures - nomenclature.....	8
2.2.3	Synthesis.....	9
2.3	Materials Characterization.....	10
2.3.1	X-ray diffraction.....	10
2.3.2	Nitrogen adsorption – BET.....	11
2.3.3	Thermogravimetric analysis.....	12
2.3.4	Electrochemical characterization.....	13
3	Experimental.....	16
3.1	Synthesis of $\delta$ -MnO <sub>2</sub> -8-F-2, $\delta$ -MnO <sub>2</sub> -8-C and $\delta$ -MnO <sub>2</sub> -8-3.....	16
3.2	Materials characterization.....	17
3.2.1	X-ray diffraction.....	17
3.2.2	Nitrogen adsorption experiments.....	17
3.2.3	Thermogravimetric analysis.....	17
3.3	Electrochemical characterization.....	18
3.3.1	Preparation of electrodes:.....	18
3.3.2	Electrochemical cycling.....	18
4	Results.....	19

4.1	Materials characterization.....	19
4.1.1	X-ray diffraction.....	19
4.1.2	Nitrogen adsorption experiments .....	23
4.1.3	Thermogravimetric analysis .....	23
4.2	Electrochemical characterization.....	24
4.2.1	Constant current .....	24
4.2.2	CV curves.....	28
5	Discussion .....	30
5.1	Materials characterization.....	30
5.1.1	X-ray diffraction.....	30
5.1.2	Nitrogen adsorption experiments .....	31
5.1.3	Thermogravimetric analysis .....	31
5.2	Electrochemical characterization.....	32
5.2.1	Constant current .....	32
5.2.2	CV curves.....	34
6	Conclusion .....	35
7	Future works .....	36
8	References.....	37
I.	Electrochemical cycling – Constant current .....	
II.	Electrochemical cycling Current Voltage .....	
III.	Parameters used during synthesis .....	
IV.	BET Ketjenblack values .....	
V.	BET Powders .....	



# 1 Introduction

---

The world is in a state of crisis when it comes to energy, as the demand for energy is increasing, but clean alternatives are still scarce. Both new and existing technologies must be refined and developed if the 2°C target from the Paris Agreement (November 2016) is to be achieved. Supercapacitors might play a role in this venture. They already have a place in key technologies such as regenerative braking, energy storage in busses in Shanghai and emergency backup generator. Supercapacitors function excellent in conjunction with batteries, and should be considered as complementary devices, used to increase efficiency and energy savings.(1) Supercapacity is a branch name and comes from the amount of energy that can stored, compared to regular capacitors. Supercapacitors can be divided into electrochemical double layer capacitors (EDLC's) (normally carbon based), and pseudocapacitors, typically based on metal oxides, hybrids and conductive polymers. Metal oxides show a lot of promise because they can store a lot of energy compared to regular EDLC's.(2) Today, the expensive but effective RuO<sub>2</sub> is the most common metal used in supercapacitors. It has a theoretical pseudocapacitance of 1358 F/g, and have already reached a specific capacitance of 720 F/g in its hydrous forms.(2) Unfortunately, it suffers from being expensive, rare, and toxic. MnO<sub>2</sub> is a promising alternative. It has a high theoretical capacitance of 1370 F/g. Unfortunately, the oxide has as many crystal structures as the author can count, and research must be done to figure out the optimal structure for capacitive properties. One of the crystal structures that show a lot of promise is the two layered Birnessite. For this material Ghodbane et al.(3) achieved 225 F/g in 0.5M K<sub>2</sub>SO<sub>4</sub>.

A lot of research has been done on MnO<sub>2</sub> based supercapacitors. Very few (if none) has come close to reach the capacitive values of RuO<sub>2</sub> (nor has anyone come close reaching the theoretical value of MnO<sub>2</sub>). There are many ways to increase Birnessite's supercapacity. A key concept is to utilize as much of the bulk as possible. When trying to reach the bulk material of MnO<sub>2</sub> based supercapacitors, it is important to consider both the conducting medium, and size of the ions. This can be tuned by selecting the right electrolyte for the capacitor. Typical electrolytes are organic, ionic, or aqueous electrolytes. Organic electrolytes don't suffer from the breakdown of water, and can thus have a higher voltage window than its aqueous counterpart (<2.3 V vs 1.23 V).(4) Unfortunately, they also have much larger solvated ions. This makes access to the narrow pores rather difficult. Organic electrolytes also have to be kept absolutely free of water, as small amounts will poison the electrolyte.(5) Aqueous electrolytes have much smaller ions.



They have much less problem utilizing the smaller pores, such as meso( $<2$  nm) and micropores(2-50nm).(2) While the storage mechanism in  $\text{MnO}_2$  based supercapacitors, allow for cations such as  $\text{Li}^+$ ,  $\text{Na}^+$ ,  $\text{K}^+$ ,  $\text{Mg}^{2+}$  to adsorb, the size of these cations differ.  $\text{Mg}^{2+}$  is known to have a low ionic radius, meaning it can more easily fit into the  $\text{MnO}_2$  surface material, than for example  $\text{Na}^+$ .(6)

Another important factor is the binder of the electrode. The amount and type will contribute a lot towards reaching high capacitance in supercapacitors. PTFE is a typical binder used during electrode production. While it does hinder electron and ion conductance, this highly depends on the ratio mixed into the electrodes. A study was performed in 2016 showing that mixing graphene into a PVDF binder could improve the total capacitance of supercapacitor electrodes.(7) No such adjustments will be made during this study.

In this thesis, composite electrodes based on  $\text{MnO}_2$  + carbon will be investigated. Two ways of creating the electrodes will be investigated. In method one, Ketjenblack is added during synthesis. The powder is named  $\delta\text{-MnO}_2\text{-8-C}$ , where C stands for carbon. In the other method,  $\text{MnO}_2$  is made without carbon during synthesis. Acetylene Black will be added during processing and mixing of the electrode slurry. These two powders are named  $\delta\text{-MnO}_2\text{-8-F-2}$  and  $\delta\text{-MnO}_2\text{-8-3}$ . These electrodes are named depending on the mixing speed used during synthesis. In both cases PTFE is used as a binder, 12% and 14 % respectively. The synthesis is based on Ghodbane et al's.(3) work, with slight modifications. Both powders will be characterized with XRD and BET. The Ketjenblack based powder will be tested with TG. The electrochemical testing will be performed using a combination of constant current (CC) and cyclic voltammetry (CV) (initially, for activation purposes), in a three-cell setup. The goal of this thesis is to investigate if  $\text{MnO}_2$  composite electrodes can be improved by adding Ketjenblack during synthesis.

## 2 Theory

This chapter is divided into three subchapters. Subchapter 2.1 is meant to introduce the reader to key concepts such as capacitance, supercapacitance and pseudocapacitance. Subchapter 2.2 gives the necessary background to understand MnO<sub>2</sub>, and its function as a pseudocapacitor. Subchapter 2.3 explains XRD, BET, TGA and how they can be used to characterize supercapacitor electrodes.

### 2.1 Capacitance

Electrochemical devices play a huge role in the modern world as secondary batteries, fuel cells and supercapacitors. In order to understand supercapacitance a brief introduction is necessary. Hence follows the background needed to grasp this intricate concept. First, there is a need to understand the concept known as capacitance. Capacitance can be understood as a materials ability to store electric charge. It has the unit Farad, with the symbol F (s<sup>4</sup>A<sup>2</sup>m<sup>-2</sup> kg<sup>-1</sup>).<sup>(8)</sup> Capacitance is defined as coulomb per volt (C/V), as seen in Equation 1:

$$C = \frac{Q}{V} \quad (1)$$

Alternatively, for parallel plate capacitors see equation 2:

$$C = \epsilon_0 * \frac{A}{d} \quad (2)$$

Where  $\epsilon_0$  is the dielectric constant,  $d$  is the distance between the two planar electrodes, and  $A$  is the surface area of the electrode. Equation 2 is only valid for planar electrodes. More advanced systems require more advanced mathematics. As seen on Figure 1, charging of the capacitor is done by applying a potential difference between the two plates. This leads to positive charge building on negative plate, and negative charge building up on the positive plate. These plates are henceforth known as electrodes. Between the electrodes is the dielectric medium. The dielectric medium prevents current to move from the negative to the positive electrode. Another benefit is the fact that the dielectric medium is polarized. This increases the

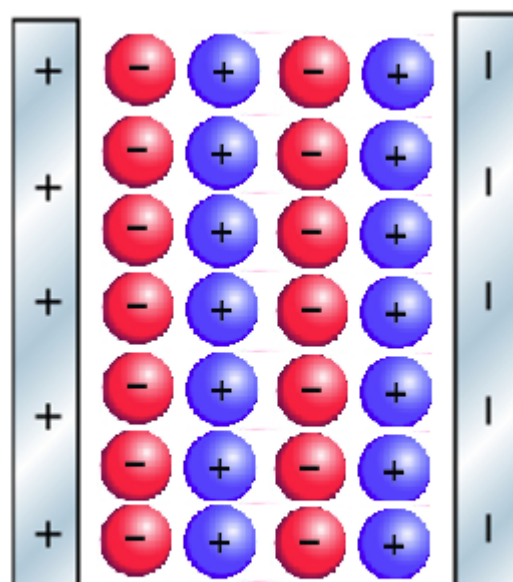


Figure 1 Charging of a parallel plate capacitor occurs as buildup of positive charge on negative plate, and negative charge on positive plate.

systems capacitance. According to Aiping yu and JiuJun Zhang (8), common dielectrics include air, oiled paper, glass and porcelain. Electrolytic capacitors differ from parallel plate capacitors as the dielectric medium is replaced by an electrolyte, which is a salt dissolved in a solvent. An electrolytic capacitor is charged by so-called double layer charging, as described in the subsequent chapter 2.1.1.

### **2.1.1 Supercapacitance – double layer theory**

Supercapacitors are electrolytic capacitors where the charging mechanism is double-layer charging of high-surface electrodes (for example porous carbon). Much like batteries and fuel cells, supercapacitors can store energy. Supercapacitors fill a niche in the field of energy storage, as they function very similarly to regular capacitors. They can charge and discharge energy rapidly, but at much higher values. They can also be cycled many times without performance loss. The high surface area of supercapacitor electrodes leads to high capacitance and reasonable energy density. For perspective; a regular capacitor holds  $10^{-3}$ - $10^{-6}$  farads, whereas a supercapacitor can hold from hundreds to thousands of Farads per device. A major difference between batteries and supercapacitors is the charge storage mechanism. While batteries use chemical/faradic reactions to store energy, supercapacitors utilize electrostatic/non-faradic mechanisms to do the same.(2) Supercapacitors function excellent in conjunction with batteries, and should be considered as complementary devices, used to increase efficiency and energy savings.(1)

The double layer model has been developed and revised several times the past decades. It was first proposed by a scientist known as Hermann von Helmholtz, and was further developed by Gouy, Chapman, Grahame and Stern. Today's theory is a combination of their and other peoples work. When an electrode comes into contact with an electrolyte, a double layer is formed. The double layer is separated from the electrode surface by an atomic distance. Champan, Gouy, Grahame and Stern noticed in their own way, that the Helmholtz model was incomplete. They separately came up with suggestions that there had to be more to the model than just the Helmholtz layer. Hence, they came up with the compact and diffuse layer. The electrode adsorbs ions in the compact layer. In the diffuse layer ions and cations are distributed evenly, driven by thermal motion. The total capacitance can be regarded as a combination of the compact layer and the diffuse layer.(2) Lately, research indicate that the measured capacitance values deviate from these models. It has been found that pore sizes are of great importance when estimating the capacitance of supercapacitor electrodes. This is especially

important when working with pores that are smaller than so called macropores (<50 nm). When working with mesopores (2-50 nm) and micropores (>2 nm), one must turn to more advanced models. This is a consequence of increased energy requirements for the ions to enter the pores. (2, 8, 9) According to Aiping Yu et al.(8) capacitance increases when pore size decrease below 1 nm. At these small pore sizes, a model known as electric wire in a cylinder can be utilized. It is clear that many factors have to be considered when choosing materials for supercapacitors.(8) The supercapacitor electrodes are typically made of the same material in both the anode and cathode. When testing supercapacitors, one tends to use a 3-electrode setup. Here only one electrode is used, along with a counter electrode (often platina), and one reference electrode. In order to reach high capacitance in a supercapacitor, one also needs to have high conductivity. Variations of carbon such as graphite or carbon black are often used as conductive additives.(10) Typically, an electrode consists of a binder, a conductive additive and a current collector. The binder is normally inert and reduces the conductivity of the electrode.(10) However, Dong et.al has bonded PVDF with graphene chemically and increased the capacity of MnO<sub>2</sub> electrodes, compared to graphene free binders.(7) For a 3-cell setup one normally calculates the capacitance using F/g, which can be seen in Equation 3.

$$C = \frac{Q}{V \cdot m} = \frac{A \cdot t}{V \cdot m} \quad (3)$$

Here C is capacitance in farad/gram, Q is the charge in ampere seconds, V is volt, m is mass in grams, and t is seconds.

### 2.1.2 Pseudocapacitance

Regular EDLC's can't store enough energy for practical applications to this date. Lately, a different variation of supercapacitors has become popular, as the need for higher energy density has become dominant. These supercapacitors are built on a mechanism known as pseudocapacitance. The mechanisms involved are reduction-oxidation (redox) reactions, intercalation and adsorption. Electrodes based on pseudocapacitive properties tend to store more energy than EDLC's.(8) Unfortunately, electrodes based on pseudocapacitance have limited cycle life and power density compared to EDLC's.(10) Typical pseudocapacitor electroactive materials are metal oxides such as RuO<sub>2</sub>, MnO<sub>2</sub>, Fe<sub>2</sub>O<sub>3</sub>, Co<sub>3</sub>O<sub>4</sub>, SnO<sub>2</sub> and NiO.(7) RuO<sub>2</sub> is a noble metal oxide and has a theoretical specific capacitance of 1358 F/g, but is both toxic and expensive.(2, 10) It is clear that cheaper and less toxic alternatives need to be developed. One of them is MnO<sub>2</sub> which will be discussed in subchapter 2.2. It should be noted

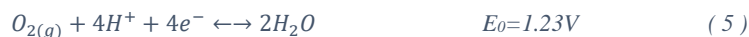
that double layer charging exists in systems based in pseudocapacitance as well. However, ion concentrations participating in double layer charging are often small in pseudocapacitors.(4)

### 2.1.3 Electrolytes

One of the key elements in a functioning supercapacitor is the electrolyte. It influences the temperature range of the supercapacitor and the voltage window. It also influences the working environment of the electrode. For example, it is important to avoid corroding materials in the cell. Equation 4 is an expression for the energy of a supercapacitor, and indicate that an increase in voltage would yield more energy than an increase in charge:

$$E = \frac{1}{2} * C * V^2 \quad (4)$$

Here E is the energy in joule, c Is the charge Q and V is volt. Equation 4 effectively proves that it is important to select an electrolyte with a high voltage window. There are three groups of electrolytes commonly used in supercapacitors, namely ionic, aqueous and organic electrolytes. Organic electrolytes have a voltage window up to 2.7 V. which is one of the reasons why they tend to be a popular choice for commercial supercapacitors. Unfortunately they suffer from being toxic and expensive, and can easily be poisoned by small amounts of H<sub>2</sub>O. (2, 5) Aqueous electrolytes are cheap and less expensive than their organic counterpart. High ionic conductivity means that the internal resistance is lowered and maximizes the specific power. Aqueous electrolytes also have small molecular diameter making it easier it easier to utilize the micro (>2 nm) and mesopores (2-50 nm).(2, 10). Unfortunately, aqueous electrolytes have a low voltage window, due to oxygen decomposition voltage of ~1.23 V and hydrogen decomposition voltage of ~0 V. This is shown in reaction 5 and 6, respectively. (11).



## 2.2 MnO<sub>2</sub> –Manganese Dioxide

### 2.2.1 Properties

Various metal oxides have already been mentioned as a substitute for the efficient, but expensive RuO<sub>2</sub>. MnO<sub>2</sub> seems to be a promising substitute. It is abundant, low cost and environmentally friendly.(7, 12) It has a theoretical specific capacitance of 1370 F/g, but this has never been achieved in practise, due to low conductivity.(7, 10). Unfortunately, literature lists very few experimental values remotely close to these values, ranging from 100-200 F/g for MnO<sub>2</sub> powders, and 700 F/g for MnO<sub>2</sub> thin film. MnO<sub>2</sub> has a very porous surface and can be synthesized into various form. Because MnO<sub>2</sub> has low electron and ion conductivity; it is even more critical with a good current collecting interface. It is also a known fact that the morphology often prevents the electrolyte to reach all parts of the material (mainly the bulk material), which in turn limits the energy yield.(2, 3) According to Ghodbane et al.(3) there are several other factors that also plays a part in limiting the electrodes, such as pore size distribution, mean manganese oxidation state and water content. Alkaline cations and chemisorbed water molecules play an important role in the redox processes during charging. (13) These reactions consist of both adsorption/desorption and intercalation/de-intercalation of electrolyte cations. This is shown in Equation 7:(13):



Where Z<sup>+</sup> is either a hydrated proton (H<sub>3</sub>O) or alkaline cation (Na<sup>+</sup>, K<sup>+</sup>, Mg<sup>2+</sup>, Li<sup>+</sup>, etc).(13) The single electron transfer changes between Mn<sup>4+</sup>/Mn<sup>3+</sup> oxidation states, according to Ghodbane et al.(3) The synthesis route plays an important part in achieving high capacitance. To that end, various crystal structures has been made, tested and charted. MnO<sub>2</sub> crystals are buildt up by [MnO<sub>6</sub>] octahedra's with shared edges, corners and faces. (3, 14) These structures are divided into several groups, depending on tunnel size and structure. Typial 1D, 2D and 3D<sup>1</sup> structures are listed in Table 1:

---

<sup>1</sup> D stands for dimension.

Table 1 Typical 1D, 2D and 3D structures of MnO<sub>2</sub>(3, 13, 15)

One dimensional	Two dimensional	Three dimensional
Nstutite ( $\gamma$ -MnO <sub>2</sub> )	Birnessite ( $\delta$ -MnO <sub>2</sub> )	Spinel ( $\lambda$ -MnO <sub>2</sub> )
Pyrolusite ( $\beta$ -MnO <sub>2</sub> )	Hollandite ( $\alpha$ -MnO <sub>2</sub> )	Todorokite
Ramsdellite (R-MnO <sub>2</sub> )		
Hausmannite (Mn <sub>2</sub> O <sub>3</sub> )		

According to Brousse et al.(16) an increase in surface area did little to increase the capacitance. Adjusting the tunnel size and structure did however provide interesting results. For example: Birnessite ( $\delta$ -MnO<sub>2</sub>) is a known 2D-layered structure. It yielded higher capacitance values compared to 1D alternatives with a higher surface area.<sup>1</sup>(16, 17) A somewhat recent study confirm these findings, showing that an increase in surface area does not necessarily increase the capacitance of the material.(18) The authors speculated that the lower electrochemical activity of  $\alpha$ -MnO<sub>2</sub> compared to  $\delta$ -MnO<sub>2</sub> was a direct result of the tunnel size and geometry.

## 2.2.2 Crystal structures

Obtaining a pure powder with only one crystal single crystal structure, is very difficult. According to Jörg H. Albering, most structural data on MnO<sub>2</sub> are obtained from single crystals measured by XRD.(14) MnO<sub>2</sub> crystallites tend to have many defects, twin domains, superstructures and partially occupied crystallographic sites. XRD is however limited when it comes to poor crystallinity. This may lead to false interpretations of the diffraction data. This then leads to incorrect structural models.(14) .

Understanding that several different structures exists, with a large variation of tunnel sizes, layers and dimensions, is key when designing MnO<sub>2</sub> for supercapacitors. MnO<sub>2</sub> consists of a

---

<sup>1</sup> 125 m<sup>2</sup>/g in the 1D material vs 17 m<sup>2</sup>/g in the Birnessite 2D material.

wide group of both natural and synthetic materials. According to Albering(14) most Birnessite materials have poor crystallinity. One example is pyrolusite ( $\beta$ - $MnO_2$ ), which can be described as the simplest variation of tunnel structured  $MnO_2$ . It consists of narrow [1x1] channels. These channels are too small for larger cations, only hydrogen and lithium can fit into the thin [1x1] channels.(14). Birnessite( $\delta$ - $MnO_2$ ) on the other hand has as mentioned a 2D-layered structure. Its stability can be attributed to the intercalated ions. They bond the structure together, as can be seen in Figure 2. Understanding the relationship between intercalation and stability of the structure is important. Cao et al.(19) performed a study on the adjusting the parameters during synthesis of  $MnO_2$ . By adjusting the amount of  $KMnO_4$  added during synthesis, they were able to increase the interlayer spacing. They also showed that increasing the number of intercalated ions too much, would decrease the specific capacitance of the material. Care needs to be taken when selecting the appropriate approach during synthesis, which will be discussed in the next chapter.(19)

### 2.2.3 Synthesis

There are many ways to synthesize  $MnO_2$  and its respective structures. A common route is the aqueous method. Ghodbane et al.(3) used a mixture of  $KMnO_4$  and  $NaOH$  mixed with an aqueous solution of  $MnCl_2 \cdot 4H_2O$ . They mixed the first solution with the last dropwise, while stirring in an ice bath. Furthermore, they statically aged the mixture at room temperature for 24h before they washed the mix and dried it at  $90^\circ C$ . They used PTFE as a binder, Acetylene Black as a conductive additive and  $MnO_2$  as current collector (3). The Birnessite acquired with this method had an interlayer distance of  $7 \text{ \AA}$ . According to Ghodbane et al.(3) it was formed by the following redox reaction:



Hydrated  $Na^+$  cations and  $H_2O$  molecules make the 2D structure stable. They achieved the following peaks during XRD characterization  $2\theta=12.2, 24.7, 36.9, 65.7$ , which they indexed as a monoclinic material with space group  $C2/m$ . The powder had a total specific surface area of  $45 \text{ m}^2/\text{g}$  and micropore surface area of  $36 \text{ m}^2/\text{g}$ . Using a  $0.5M K_2SO_4$  electrolyte, they achieved a capacitance of  $225 \text{ F/g}$ .(3) Figure 2 illustrates a Birnessite structure with a monoclinic space group.(3, 14) The finished powder typically consists of several other phases as well. Among others, pyrolusite, Hausmannite ( $Mn_2O_3$ ) and Feitknechte should be mentioned.(3) Typically, Hausmannite forms at elevated temperatures, so temperature control is key. However, several



methods can be used to improve the Birnessite formation, such as applying an electric field to improve the lattice structure.(20)

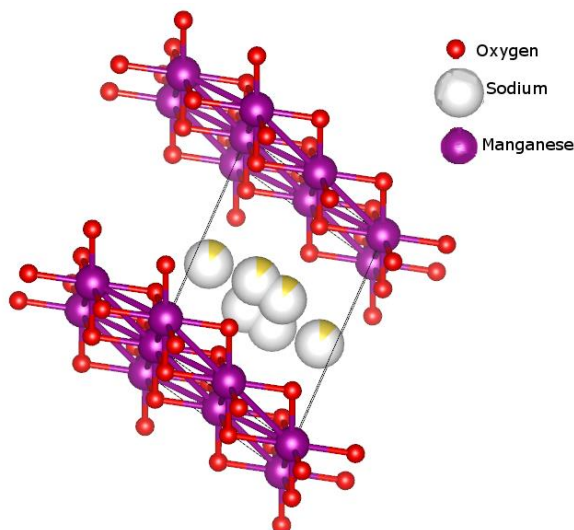


*Figure 2 Illustration of Birnessite with the unit cell parameters  $a=5.174\text{Å}$ ,  $b=2.850\text{Å}$ ,  $c=7.336\text{Å}$  and  $\beta=103.18^\circ$ , space group  $c2/m$ , monoclinic. Sodium ( $\text{Na}^+$ ) represents the cation layer.*

## 2.3 Materials Characterization

### 2.3.1 X-ray diffraction

The name X-ray diffraction (XRD) or Röntgenstrahlung comes from a German Scientist known as Wilhelm Röntgen. X-rays are high-energy electromagnetic radiation. They can penetrate much deeper into materials than regular light waves.(21) The radiation has wavelengths between  $\sim 0.1\text{-}100\text{Å}$ . (22) This comes in handy when working with powders and other crystalline materials. XRD is considered a fingerprint technique, which means that the exact crystal structure can be matched in respective databases. The technique is based on the fact that X-rays are scattered by atomic planes. In the presence parallel planes, the scattered X-rays may interfere constructively, depending on the angle of the reflected beam,  $\theta$ , and the distance between the planes. Diffraction angle is an important measurable feature. It is the angle between the diffracted beam and the transmitted beam. This angle is always  $2\theta$ .(21) Diffraction can be most easily observed when the wavelengths are of the same order as the slit separation.(23). The condition for constructive interference is expressed by Bragg's law:

$$2d * \sin \theta = n\lambda \quad (9)$$

Here  $d$  is the distance between atomic layers in a crystal,  $\lambda$  is the wavelength of the x-ray beam,  $n$  is an integer and  $\theta$  is the incident angle. When the conditions for constructive interference are met, the resulting peak in the X-ray diffractogram can be used to determine the value of  $d$ . X-rays are generated by accelerating electrons towards a metal target, with Cu as one of the most commonly used. During powder diffraction measurements, one uses a fixed wavelength, and a variable angle. The characteristic wave length of a Cu target is  $\lambda=1.54 \text{ \AA}$ .(21) The Scherrer equation is an important equation and relates the broadening peak to the mean crystallite dimension (thickness of the crystallite)  $\tau$ , as seen in Equation 10

$$\tau = \frac{K*\lambda}{\beta_{\tau}*\cos\theta} \quad (10)$$

Where  $\beta_{\tau}$  is the full width at half maxima which is given by (B-b), where B is the total width of the observed diffraction line at its half intensity maximum, and b is the instrumental broadening. K is the shape factor.  $\theta$  is the Bragg angle,  $\lambda$  is the x-ray wavelength.(24)

### 2.3.2 Nitrogen adsorption – BET

Brunauer-Emett-Teller (BET) theory describes how physical or chemical adsorption of gas molecules occur on a solid surface. It is used for the interpretation of nitrogen adsorption data. The technique is used to determine the specific surface area of materials. BET-theory can be considered an extension of Langmuir theory – Ideal Localized Monolayer Adsorption.(25) According to Sing et al.(25) the model normally referred to as Langmuir, is that of a scenario where a plane surface has only one kind of elementary site. This means it can only hold one adsorbed molecule. However, this limits the theory to a monomolecular surface. Figure 3 illustrates the various randomly adsorbed stacked molecules. If the relative pressure  $p/p^{\circ}$  is increased, the gas penetrates deeper into the material.

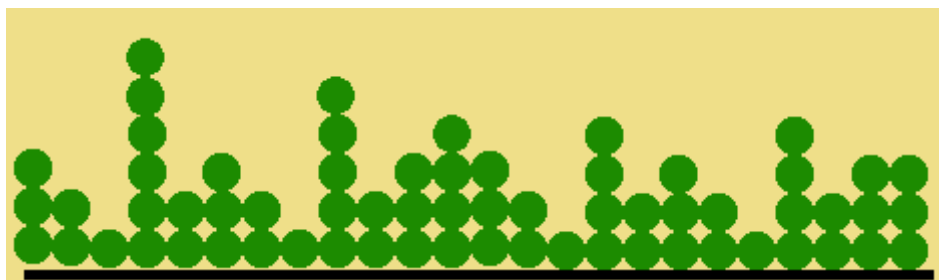


Figure 3 - BET model of multilayer adsorption.

Physisorption is based on relatively weak van der Waals forces, and thus it takes little energy to remove physisorbed species from a solid surface. Physisorption is reversible, so BET is in principle non-destructive. Physisorption gives information about surface area, pore size and pore size distribution.(26) The BET model is based on a set of assumptions(25):

1. Adsorption takes place on an array of fixed sites.
2. The sites have the same energy.
3. There are no lateral interactions between adsorbed molecules.

One may then calculate the specific surface area of a solid material using variations of the BET equation (Equation 11) and a set of data points collected during measurements.

$$\frac{x}{V(1-x)} = \frac{1}{V_m * C_{BET}} + x * \frac{C_{BET}-1}{V_m * C_{BET}} \quad (11)$$

- V= Volume of adsorbed molecules.
- V<sub>m</sub>= monolayer volume
- C<sub>BET</sub> = BET constant (related to adsorbate adsorbent interaction strength)
- x= relative pressure p/p<sub>0</sub>(26)

Luckily, most modern equipment for BET measurements, automatically calculate the results in advance, so the equation is rarely needed in practise. The results may be influenced by external factors such as varying temperature and atmospheric changes. Also, the accuracy of the test is limited to the pore radius of the adsorbent gas (N<sub>2</sub>/O<sub>2</sub>/Kr/Ar), which have an adsorption cross section of about 0.14-0.23nm.(27, 28)

### 2.3.3 Thermogravimetric analysis

TGA measures change of mass in relation to the change of temperature over time. The technique combines control of the atmosphere by various purge gases, (Air, Argon, Nitrogen etc.) with a steady temperature change. The change of mass gives information about phase changes, such as water to gas. The measurements may be influenced by important factors such as atmospheric effects and secondary reactions according to Bruce. Et al.(29) Buoyancy is also a factor that has to be considered. This is an upward force on the sample produced by the density of the atmosphere inside the TGA balance. This may vary with both temperature and rate of temperature change. Effects of buoyancy may be observable during the start of a heating segment.(29) In most new TGA's this problem has been removed. It can still be seen in old TGA's.

### 2.3.4 Electrochemical characterization

Electrochemical cycling is an important tool that can help to describe the energy storage capability of supercapacitor electrodes. Basically, one uses electrochemical reactions to charge the powder. These charges are normally measured as capacitance. Various designs exist to measure capacitance. A typical setup is the three-electrode cell, consisting of an electrode with an active material, a counter electrode and a reference electrode.(30) The cell is most often used in combination with a potentiostat. The potentiostat generates a specific cell voltage, that may be constant or change with time, with respect to the working electrode.(2, 31) When an electrode is polarized in an electrolyte, mass transfer occurs, either because of double layer charging, or as a consequence of a faradaic reaction. One quantifies this motion using a unit known as flux density, which is defined by Equation 12:

$$j_i = \frac{1}{A} * \frac{dn_i}{dt} \quad (12)$$

Here  $dn_i$  is the number of moles  $i$ , that crosses a surface area  $A$  in the time interval  $dt$ .(31) Flux density is the same as the product of the concentration of a solute and average velocity in the direction of motion. The movement of the solution can be sorted into three different mechanisms of transport, namely convection, diffusion, and migration. Migration is the effect of electrical potential. Diffusion is the effect of the activity of concentration gradients. Convection is the effect of pressure and movement in the liquid.(31, 32) . Migration is normally circumvented by adding a supporting electrolyte. The effects of natural convection are often quite small and can be ignored during most experiments. Thus, in most practical systems, one only need to considers diffusion, which can be calculated using Ficks first and second law.(31, 32) During electrochemical cycling there is always some cell resistance. Cell resistance occurs due to the solution resistance between the electrodes.(32) Cell design is important to limit the resistance of the cell. A typical design has a relatively short distance between the working electrode and the reference electrode. The cell should be made by an inert material, for example Teflon.

#### 2.3.4.1 Cycling of MnO<sub>2</sub>

Electrochemical cycling often affects the crystal structure of the supercapacitor materials. Ghodbane et al.(17) did a study where they looked at changes of crystal structures during charging and discharging of supercapacitor electrodes with various structures. Figure 2 in chapter 2.2.3 illustrates that Na<sup>+</sup> cations have intercalated in the Birnessite material during

synthesis. When you charge/discharge the supercapacitor electrodes, cations will adsorb into the material. Ghodbane et al.(17) noticed a very visible shift in d-spacing during X-ray diffracting, indicating insertion and desinsertion of hydrated alkali cations from the electrolyte, into the lattice. The observed swelling had different observed CV peaks during cycling, which could be attributed to the different ionic radii of  $K^+$  vs  $Li^+$ .(17)

### 2.3.4.2 Cyclic voltammetry

Cyclic voltammetry is used to investigate redox reactions in 3-cell setups. Figure 4 illustrates a typical CV curve. This CV curve follows the IUPAC convention. Here the x-axis is imposed potential V, and the y-axis is the response in the form of current, typically mA.(33)

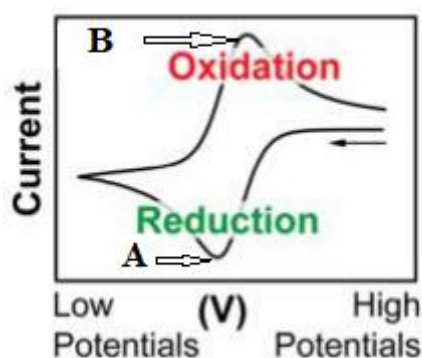


Figure 4 Illustration of a CV curve. Borrowed and edited from Elgrishi et al. (33)

The Nernst equation (Equation 13) is typically used to calculate the changes happening to a CV curve:

$$E^{\text{rev}} = E = E^0 + \frac{RT}{F} * \frac{\ln(Ox)}{\ln(red)} \quad (13)$$

Here  $E^{\text{rev}}$  is the reversible potential,  $E^0$  is the standard potential, T is the temperature in Kelvin, F is Faraday's constant. The cation is slowly reduced and is thus depleted near the electrode. Once the peak cathodic current has been reached as illustrated by point A in Figure 4, the reaction is driven by. At the surface of the electrode a so called diffusive layer forms, and grows during the negative scan. The mass transport is thus diffusion limited and can be calculated by Fick's law. (33) When the cycle shifts towards oxidation, the scan direction is reversed. The reverse happens the cation density at the electrode increases.(33) Ghodbane et al.(17) investigated the CV curves of Birnessite and found a reversible deintercalation/intercalation process of  $Na^+$  cations during cycling. They also found that during discharge, a decrease in  $Na^+$

cations from the Birnessite was compensated by intercalation of H<sub>2</sub>O. During reduction, the opposite happens, and the interlayer spacing shrinks.(17)

### 3 Experimental

---

All the chemicals were of analytical grade, and acquired from Sigma-Aldrich. They have been used without purification and modifications.

#### 3.1 Synthesis of $\delta$ -MnO<sub>2</sub>-8-F-2, $\delta$ -MnO<sub>2</sub>-8-C and $\delta$ -MnO<sub>2</sub>-8-3

Wet synthesis was used to synthesize  $\delta$ -MnO<sub>2</sub>. Two solutions were made following a modification of Ghodbane's work:(3, 17).

- Solution A: 0.02 mole KmNO<sub>4</sub> (99.2%), and 0.30 mole NaOH, 200ml.
- Solution B: 0.0560 mole MnCl<sub>2</sub>\*4H<sub>2</sub>O (~99%), 200 ml.

The solutions were placed in recrystallization beakers and stirred until 2-4 °C was reached. Fresh ice was continuously resupplied during mixing. The solutions were mixed by titration or pouring of solution B into solution A, at rates given in Table 2. (A complete list of parameters used during synthesis can be found in Appendice III – Parameters used during synthesis).

Table 2 List of the respective mixing speeds of  $\delta$ -MnO<sub>2</sub>-8-F-2,  $\delta$ -MnO<sub>2</sub>-8-3 and  $\delta$ -MnO<sub>2</sub>-8-C.

Material	$\delta$ -MnO <sub>2</sub> -8-3	$\delta$ -MnO <sub>2</sub> -8-F-2	$\delta$ -MnO <sub>2</sub> -8-C.
Method	Titration	Pouring	Pouring with carbon <sup>1</sup>
Mixing speed	(0.02-0.05ml/s)	10-15ml/s	10 ml/s
Total time	~2h	~20 s	20 s

For  $\delta$ -MnO<sub>2</sub>-8-C Ketjenblack (1435m<sup>2</sup>/g)<sup>2</sup> was mixed into solution A, and stirred intensely until the carbon mixed with the solution. All solutions were left to crystallize for 24h. The solutions

<sup>1</sup> Carbon was mixed into solution A prior to mixing with solution B, with vigorous stirring.

<sup>2</sup> Acquired from SINTEF, Appendice IV - BET Ketjenblack values.

were filtrated and washed until pH 7 was reached. The remaining powder was dried at 60°C for 18h and crushed into fine particles (in a regular heating furnace). The materials were named depending on how they were synthesized.<sup>1</sup>

## **3.2 Materials characterization**

XRD and BET was used to characterize all the synthesized powders. TGA was used to measure carbon loss of  $\delta$ -MnO<sub>2</sub>-8.

### **3.2.1 X-ray diffraction**

The sample was placed into a clean sample holder, and scanned with D-8 Focus X-ray diffractometer for 80 minutes, between 10-75 degrees 2 $\theta$ . The resulting XRD chart was then analysed by the help of EVA fingerprint technique. The software was used to identify the crystal structures in the powder.

### **3.2.2 Nitrogen adsorption experiments**

Nitrogen adsorption experiments were conducted by a 3 Flex 3500 surface area, porosity and chemisorption analyser. The surface area was determined by the Brunauer Emmett Teller method (BET) for the powders  $\delta$ -MnO<sub>2</sub>-8-(2,3) and  $\delta$ -MnO<sub>2</sub>-8-C. The samples were degassed (N<sub>2</sub>, 110 °C) for 12h, with Degas Smart Prep for 3 Flex 3500. Flex 3500 Chemisorption analyser was used to determine the surface area using a five-point BET method, at -195 °C.

### **3.2.3 Thermogravimetric analysis**

Thermogravimetry was run on a  $\delta$ -MnO<sub>2</sub>-8-C sample (0.14981mg), in a Netzsch STA 449 C Jupiter thermal analyser. A background was performed, then TG was run from 25-600 °C, at 10° C/min in synthetic Air (70/30, O<sub>2</sub>/N<sub>2</sub>).

---

<sup>1</sup> The naming works as follows  $\delta$ -MnO<sub>2</sub>-8 says that we are working with a Birnessite material. The number in the end, explains the number in the series (for ex, three variations of  $\delta$ -MnO<sub>2</sub>-8-3 have been made). The C, stands for carbon, and F stands for fast mixing. This naming was made to systemize the powders during synthesis.



### 3.3 Electrochemical characterization

Electrodes were prepared by a processing step, and then cycled in order to measure the capacitance of the electrodes.

#### 3.3.1 Preparation of electrodes

$\delta$ -MnO<sub>2</sub>-8-F-2 and  $\delta$ -MnO<sub>2</sub>-8-3 was made mixing PTFE (12%), MnO<sub>2</sub> (73%), Acetylene black (15%) and a small amount of ethanol. The mix was milled (25Hz) for 1 hour. The mixture was then applied to Toray Carbon Fiber Paper (TGP-H-090, 0.28mm) by hand. The electrodes were left to dry for ~18 h, and placed in a Vacuum drying chamber – VD 23 for 6 hours (60 °C, 0.01mbar).  $\delta$ -MnO<sub>2</sub>-8-C was made using PTFE (14%), MnO<sub>2</sub> (61%), Ketjenblack (25%) and slightly more ethanol as a solvent.

#### 3.3.2 Electrochemical cycling

*Table 3 Cycling parameters.*

Ampere per gram (A/g)	Cycle(long)	Cycle(short)
0.1	50	10
0.2	50	10
0.5	50	10
1.0	1000	10
2.0	50	10
0.1 <sup>1</sup>	5	-

A standard three electrode cell was used in combination with Biologic VMP 3 potentiostat. The reference electrode was a saturated Ag/Cl reference electrode and the counter electrode was a platinum-Iridium spiral electrode (determined resistance: 20mOhm)(34). 1 M MgSO<sub>4</sub> was purged with N<sub>2</sub> gas for 30-60 minutes before use. The electrode was wetted for 6 hours and OCV was measured simultaneously. Nitrogen purged the cell at all times. Cyclic voltammetry (50 cycles, 50mv/s) and constant current (see Table 3) was then applied to the cell. Electrode voltage was set between 0-0.9 V. Cyclic voltammetry was reapplied after testing at 5, 10, 20, 50, 100 mv/s, but only for the long cycle.

<sup>1</sup> Only performed for the long cycle test of  $\delta$ -MnO<sub>2</sub>-8-F-2

## 4 Results

The result section is divided into a material characterization section, and an electrochemical characterization section.

### 4.1 Materials characterization

#### 4.1.1 X-ray diffraction

This section shows three tests of the powders used during this thesis. The first two figures are powders with Acetylene Black mixed in at a later stage, whereas the last powder,  $\delta$ -MnO<sub>2</sub>-8-C has Ketjenblack mixed in prior to XRD scans. The Birnessite peaks are summarized in Table 4.

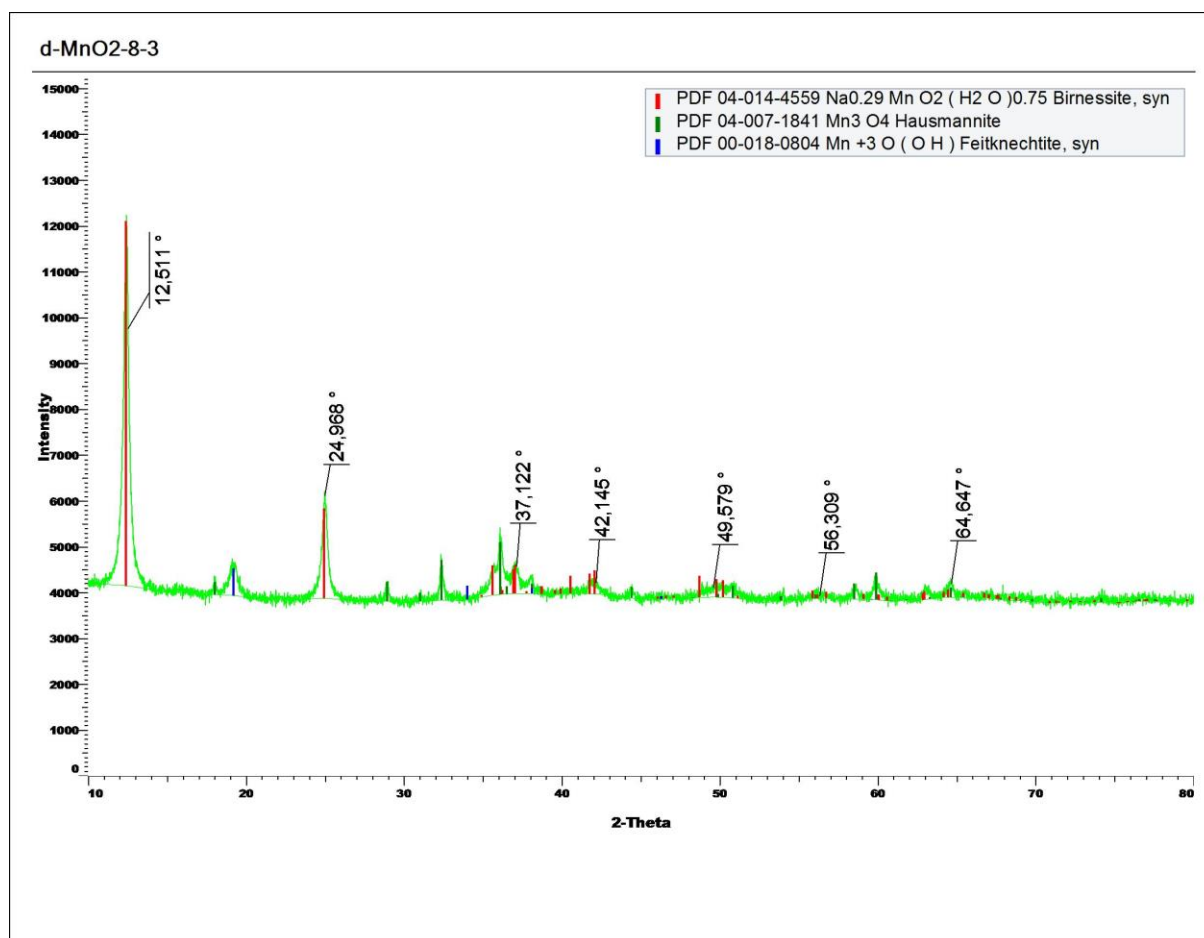


Figure 5 XRD chart showing typical Birnessite (red) peaks at  $2\theta = 12.5, 25.0, 37.1, 64.6$ . Hausmannite (green) has also been identified. Feitknechtite (blue) is believed to be observed at  $2\theta = 19.5$ .

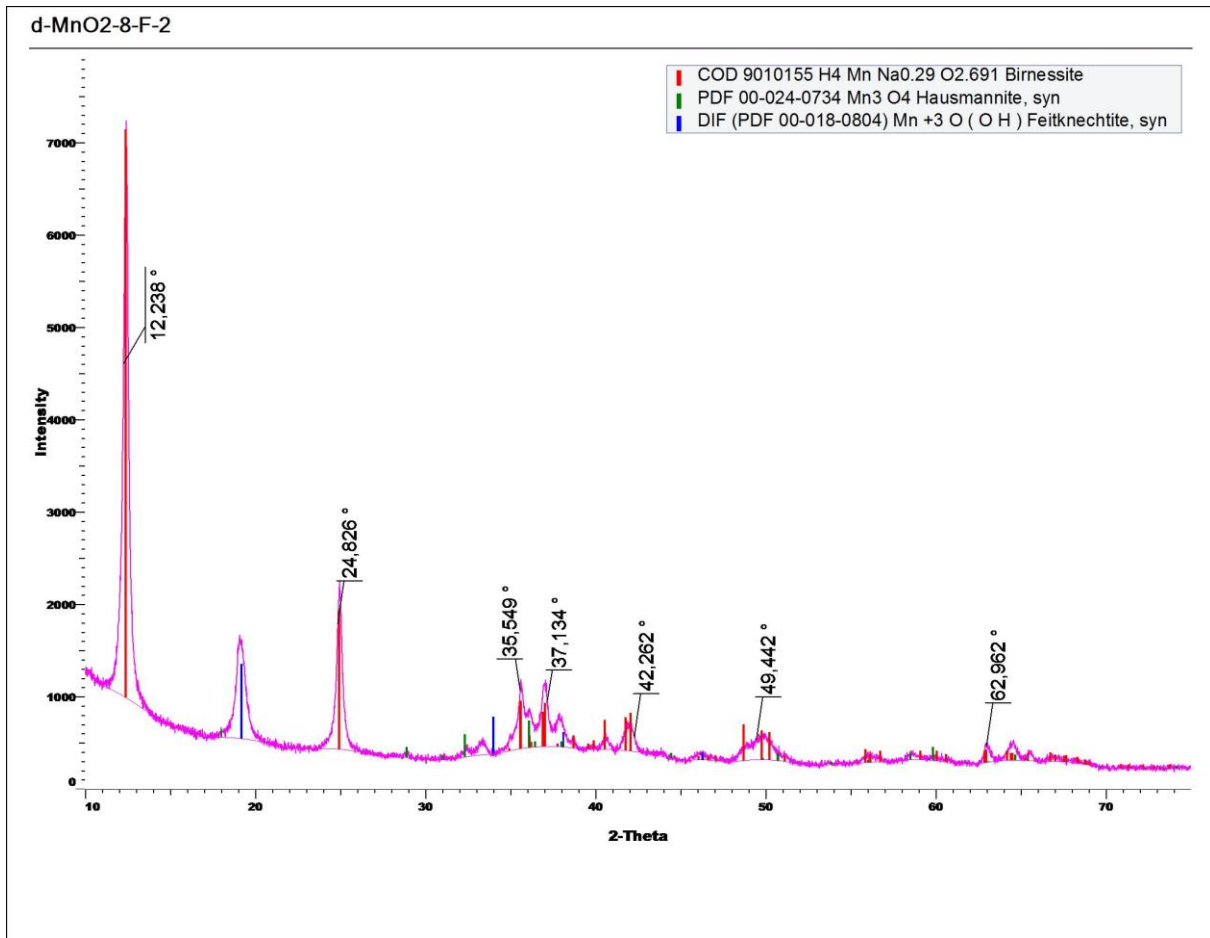


Figure 6 XRD chart showing typical Birnessite (red) peaks at  $2\theta = \sim 12.2, 24.8, 37.1, \sim 63$ . Feitknechtite (blue) is seen around  $2\theta = 19.5$ , and Hausmannite (green). Other Birnessite peaks are also observed at  $2\theta = 35.5, 42.3, 49.4$ .

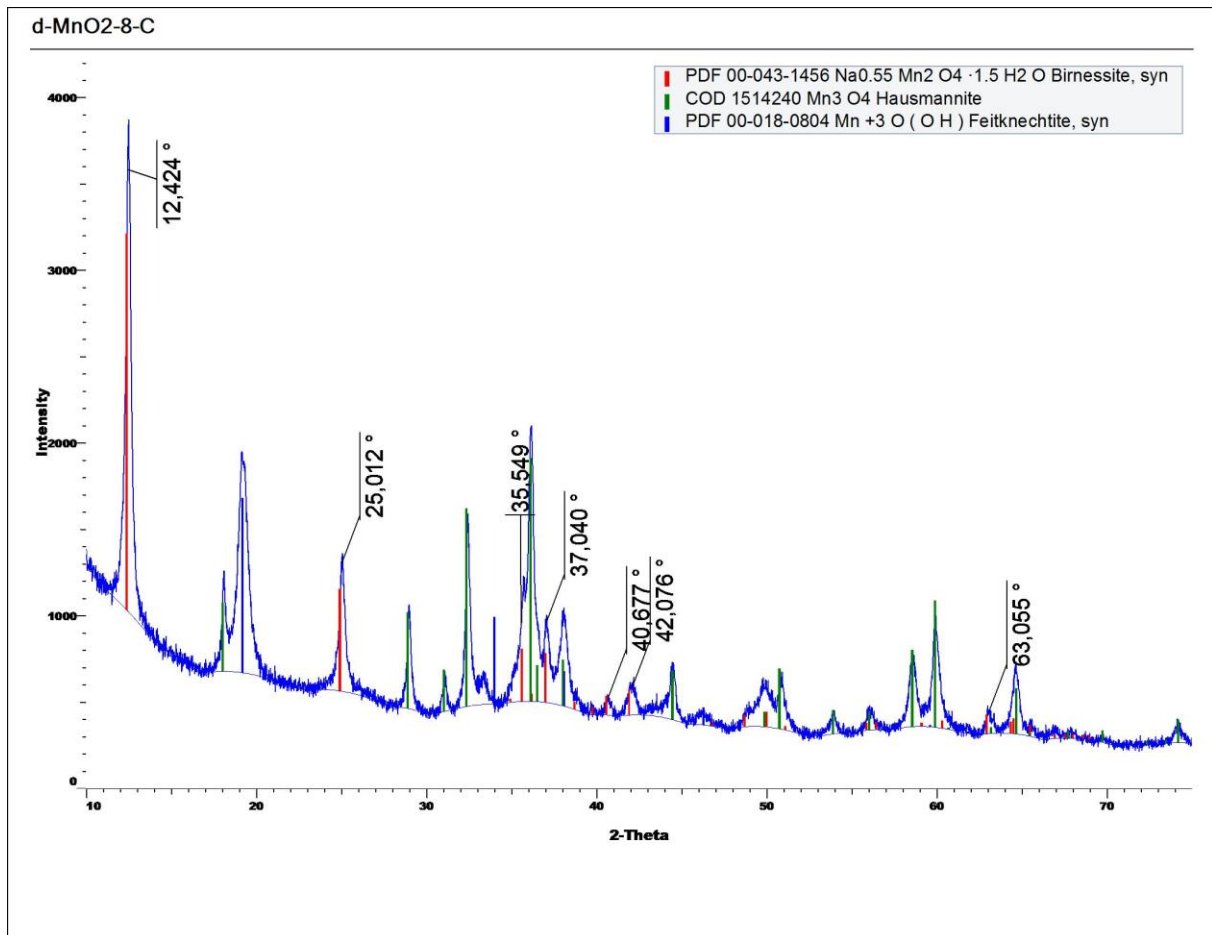


Figure 7 XRD chart showing typical Birnessite (red) peaks at  $2\theta=12.4, 25, 37, 63$ . Other Birnessite peaks seem to be  $2\theta=35.5, 40.7, 42.1$ . Hausmannite seems clearer here than on the other XRD-charts. Feitknechtite is identified at around  $2\theta=19.5$ .

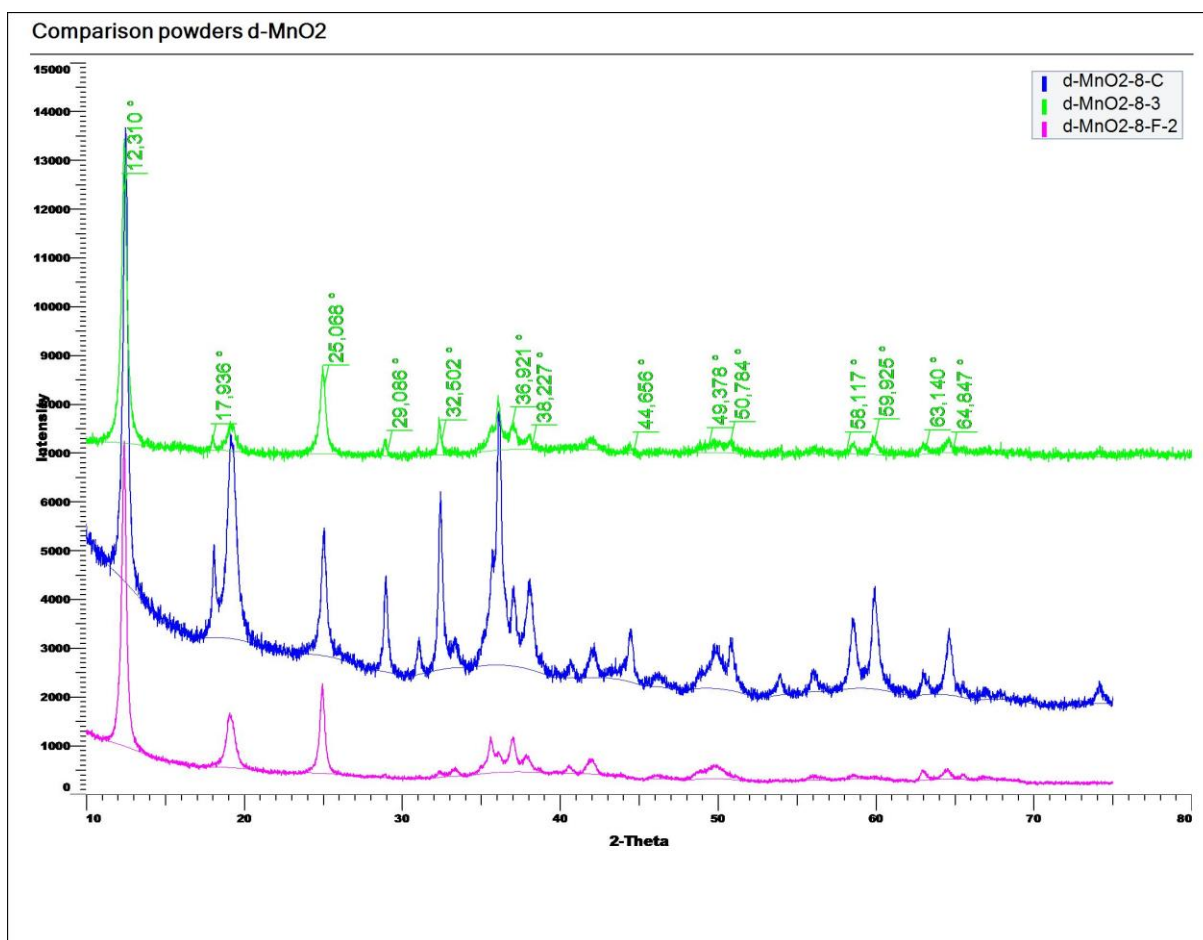


Figure 8 The three XRD charts are placed here to illustrate the difference in crystal structure. Most of the structures seem to be apparent on all XRD charts. However, as seen on Figure 5,6,7, there are slight variations in  $2\theta$ .

Table 4 lists the observed Birnessite peaks, and their relative d-spacings in Ångström.  $K_{Cu}=1.5406$ . Equation 9: Bragg's law has been used to calculate the d-spacings.

Table 4 The table lists the most easily visible Birnessite peaks identified with the EVA software. Peaks identified by hand.

Birnessite Peaks $2\theta$								
n	1	2	3	4	5	6	7	8
$\delta$ -MnO <sub>2</sub> -8-3	12.5	25.0	36.0	37.1	41.9	42.1	49.6	64.6
d-spacing Å	7.076	3.559	2.493	2.421	2.154	2.145	1.836	1.442
$\delta$ -MnO <sub>2</sub> -8-F-2	12.2	24.8	35.5	37.1	42.3	59.4	62.9	-
d-spacing Å	7.249	3.587	2.527	2.421	2.135	1.555	1.476	-
$\delta$ -MnO <sub>2</sub> -8-F-C	12.4	25.0	35.5	37.0	40.7	42.1	56.0	63.0
d-spacing Å	7.132	3.559	2.527	2.428	2.215	2.145	1.641	1.474

### 4.1.2 Nitrogen adsorption experiments

BET 5-point fingerprint technique has been used to measure the surface area of the powders used in the electrodes in this work. Table 5 shows the relations of surface area, pore size, and key parameters used during testing.

Table 5 BET 5-point fingerprint technique of  $\delta$ -MnO<sub>2</sub>-8-F-2,  $\delta$ -MnO<sub>2</sub>-8-3,  $\delta$ -MnO<sub>2</sub>-8-F-C.

Sample ID	Degas time	Degas temperature	BET SA	Pore size (BJH)
<b><math>\delta</math>-MnO<sub>2</sub>-8-F-2</b>	12h	110°C	46 ± 0.46 m <sup>2</sup> /g	2.068 nm
<b><math>\delta</math>-MnO<sub>2</sub>-8-3</b>	12h	110°C	66 ± 0.34 m <sup>2</sup> /g	21.329 nm
<b><math>\delta</math>-MnO<sub>2</sub>-8-F-C</b>	12h	110°C	408 ± 3.8 m <sup>2</sup> /g	2.065 nm
<b>Ketjenblack</b>	-	-	1435 ± 4.84 m <sup>2</sup> /g	-

### 4.1.3 Thermogravimetric analysis

TGA data was gathered with Netzsch Sta 449 C. As seen in Figure 9, small peak was found at 60 °C. A small drop in mass occurred at around 100°C, giving the expected mass loss of water as well as a large loss of weight from 325°C to 515°C, 25 wt%, the latter being loss of carbon.

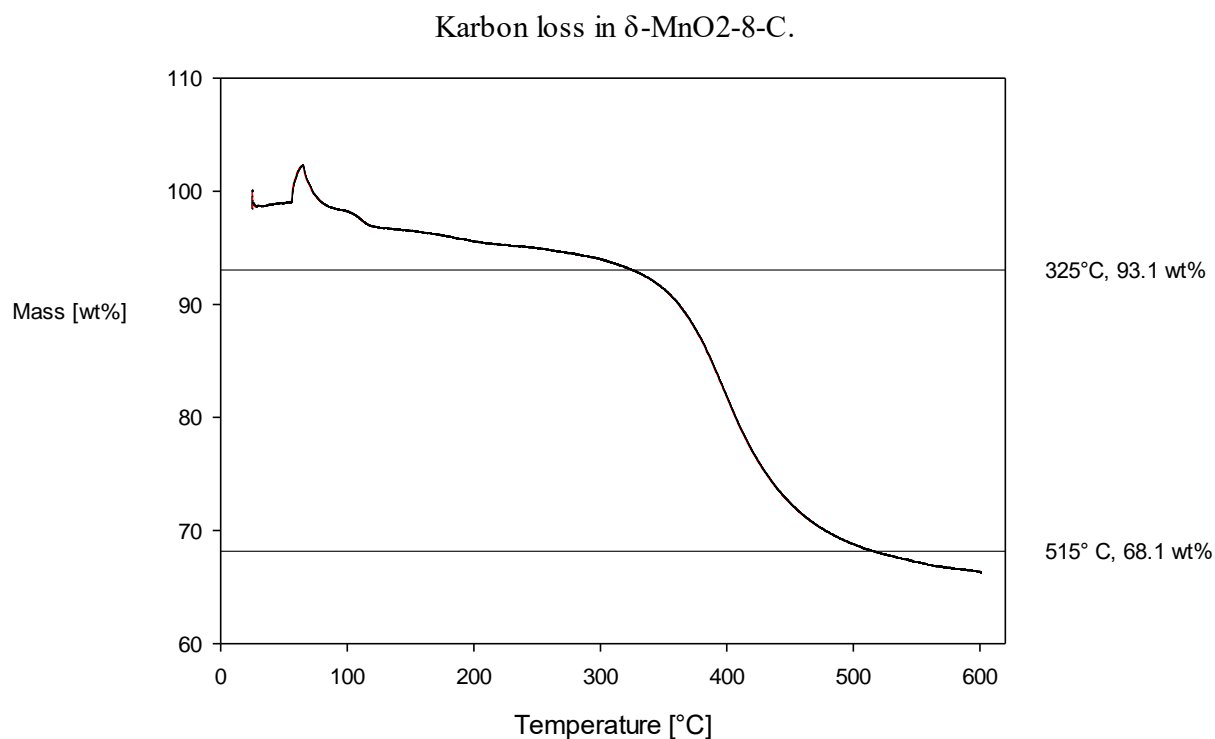


Figure 9 TGA measurement of  $\delta$ -MnO<sub>2</sub>-8-C. Mass loss estimated from graph to be approximately 25 wt% carbon.

## 4.2 Electrochemical characterization

The following few pages presents a table and several graphs that show measurements at 0.1 A/g, 0.2 A/g 0.5 A/g, 1.0 A/g, 2.0 A/g of both short and long cycles. Notable values as high as 501 F/g for  $\delta$ -MnO<sub>2</sub>-8-C-4, and 474 F/g for  $\delta$ -MnO<sub>2</sub>-8-F-2 at 0.1 could be observed during cycling. Section 4.2.1 shows results from constant current measurements. Section 4.2.2 shows CV curves for the electrodes with the highest capacitance values. Table 6 lists all the measurements done with CC and the rate capability.

### 4.2.1 Constant current

Table 6 All the electrodes tested + their respective capacitance values at 0.1, 0.2, 0.5, 1.0 and 2.0 A/g. (2<sup>th</sup> and 9<sup>th</sup> cycle in the short electrodes), + rate capability.

<i>Capacitance (F/g) at second and last cycle.</i>						
<b>Electrode</b>	<b>0.1 A/g</b>	<b>0.2 A/g</b>	<b>0.5 A/g</b>	<b>1.0 A/g</b>	<b>2.0 A/g</b>	<b>Rate capability</b>
<b><math>\delta</math>-MnO<sub>2</sub>-8-3-1</b>	330/389	363/371	339/341	308/308	278/278	71 %
<b><math>\delta</math>-MnO<sub>2</sub>-8-3-5</b>	304/365	351/358	327/327	296/294	253/253	69 %
<b><math>\delta</math>-MnO<sub>2</sub>-8-C-2</b>	425/447	273/272	247/248	235/236	210/210	47 %
<b><math>\delta</math>-MnO<sub>2</sub>-8-C-3</b>	331/440	382/392	316/316	238/234	136/138	31 %
<b><math>\delta</math>-MnO<sub>2</sub>-8-C-4</b>	438/501	433/446	405/408	379/378	347/340	68 %
<b><math>\delta</math>-MnO<sub>2</sub>-8-C-6</b>	369/430	391/393	352/349	319/318	287/287	67 %
<b><math>\delta</math>-MnO<sub>2</sub>-8-F-2</b>	440/474	409/403	350/340	306/236	-	50 %

The standard deviation for the 9<sup>th</sup> cycle is calculated for the Ketjenblack electrodes, using Equation 13

$$\sigma = \sqrt{\frac{1}{N-1} * \sum_{i=1}^N (x_i - \bar{x})} \quad ( 14 )$$

Where N= number of samples, xi = sample, and  $\bar{x}$  is the average of the four carbon electrodes.

This gives the following capacitances + standard deviation:

- 0.1 A/g → 455 ± 32 F/g
- 0.2 A/g → 376 ± 74 F/g
- 0.5 A/g → 330 ± 67 F/g
- 1.0 A/g → 292 ± 70 F/g
- 2.0 A/g → 244 ± 88 F/g

#### 4.2.1.1 Constant current - long cycle

Figure 10, 11, 12, 13 show cycling of  $\delta\text{-MnO}_2\text{-8-F-2}$  for 0.1, 0.2, 0.5 and 1.0 A/g respectively.

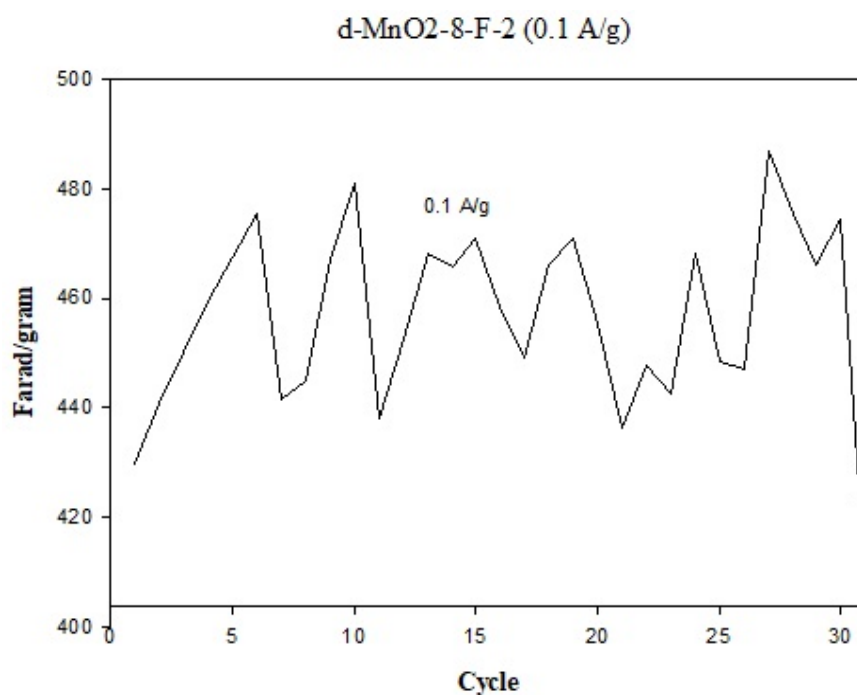


Figure 10 First 30 cycles of discharge at 0.1 A/g. The capacitance increases until cycle 30.

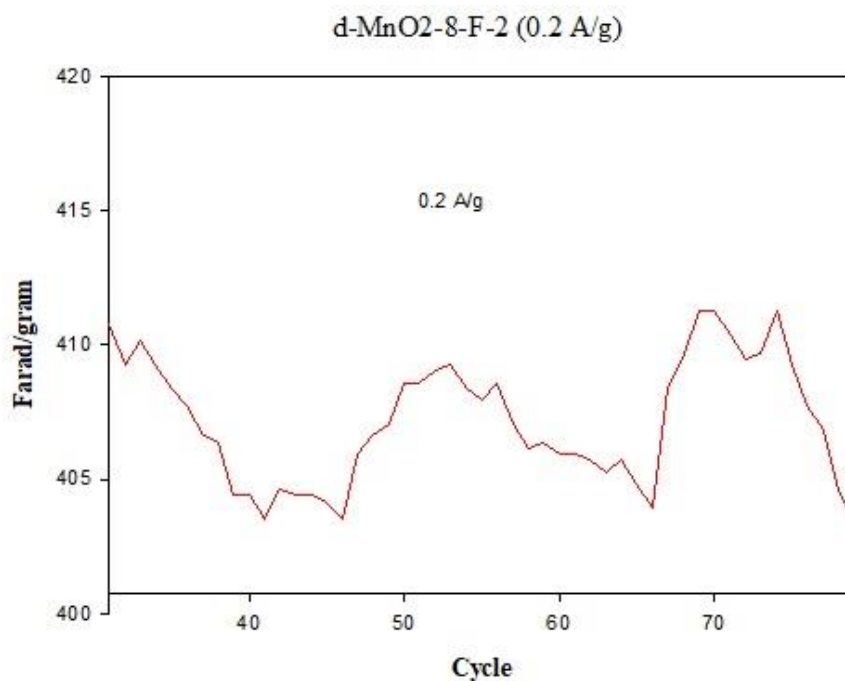


Figure 11 Cycle 30-80 of the long-cycled electrode, shows the capacity to still fluctuate at 0.2 A/g, but less than during the first 30 cycles.



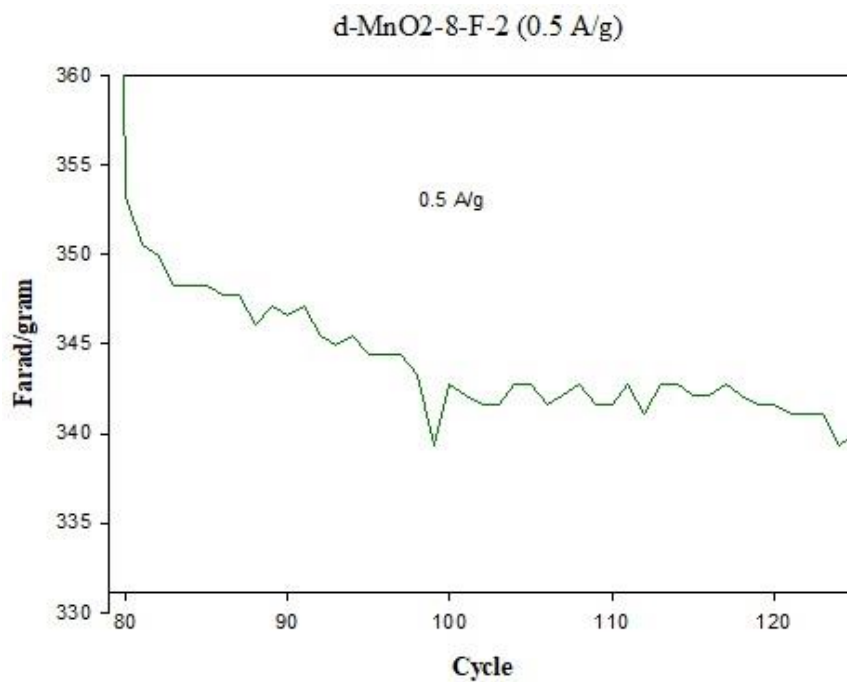


Figure 12 Cycle 80-125 - the electrode seems to stable, but is slowly diminishing in capacitance.

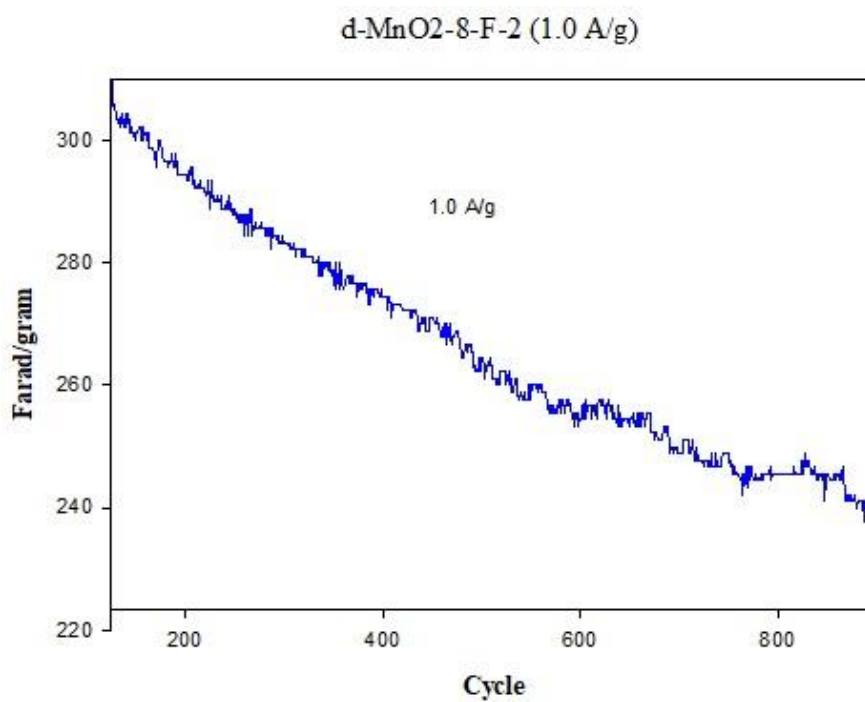


Figure 13. The electrode has lost 22.74% capacitance from cycle 125 till cycle 979, at 1.0 A/g-

#### 4.2.1.2 Column charts - short cycles

The following column charts represents the two electrodes with highest capacitance, one for Acetylene Black and one for Ketjenblack. The remaining diagrams can be found in Appendice I - Electrochemical cycling - Constant current.

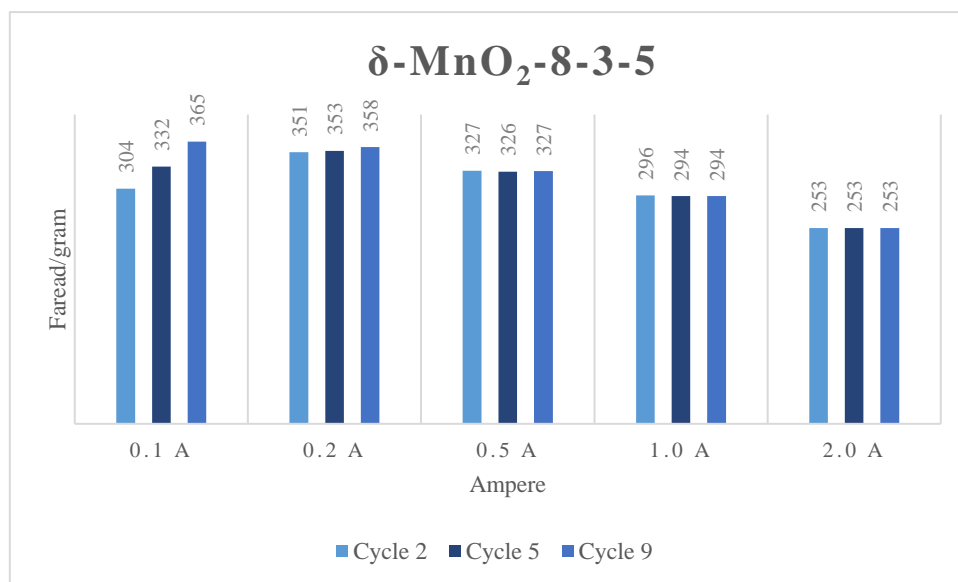


Figure 14 Capacitance values during discharge at 2, 5, 9 cycles on 0.1, 0.2, 0.5, 1.0, 2.0 A/g for  $\delta$ -MnO<sub>2</sub>-8-3-5.

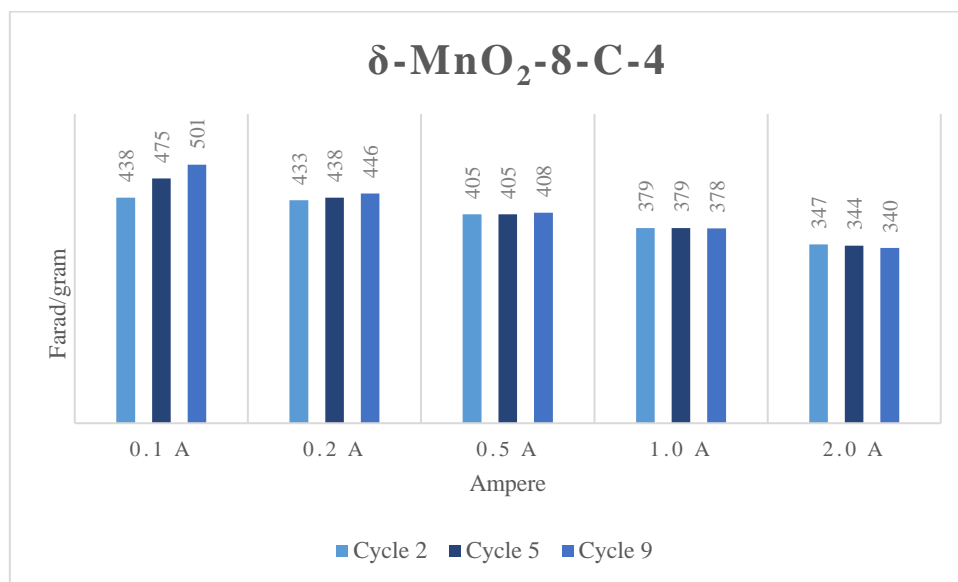


Figure 15 Capacitance values during discharge at 2, 5, 9 cycles on 0.1, 0.2, 0.5, 1.0, 2.0 A/g for  $\delta$ -MnO<sub>2</sub>-8-C-4.

### 4.2.2 CV curves

The following CV curves are shown to illustrate changes in the material during charge/discharge for the electrodes  $\delta\text{-MnO}_2\text{-8-F-2}$ ,  $\delta\text{-MnO}_2\text{-8-3-5}$  and  $\delta\text{-MnO}_2\text{-8-C-4}$ .

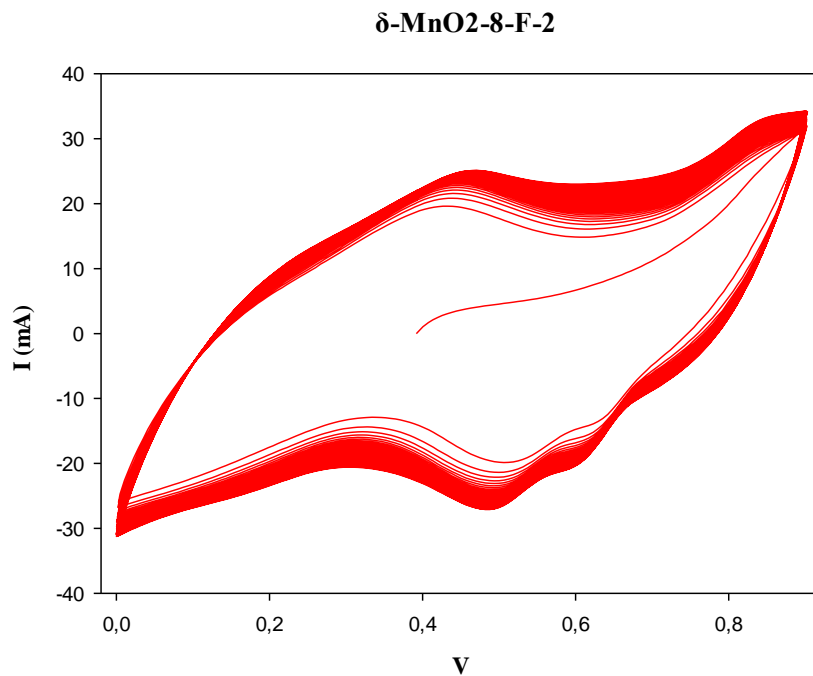


Figure 16 A cathodic peak can be observed at 0.48V, and a similar anodic peak is observed at 0.44V, for  $\delta\text{-MnO}_2\text{-8-F-2}$

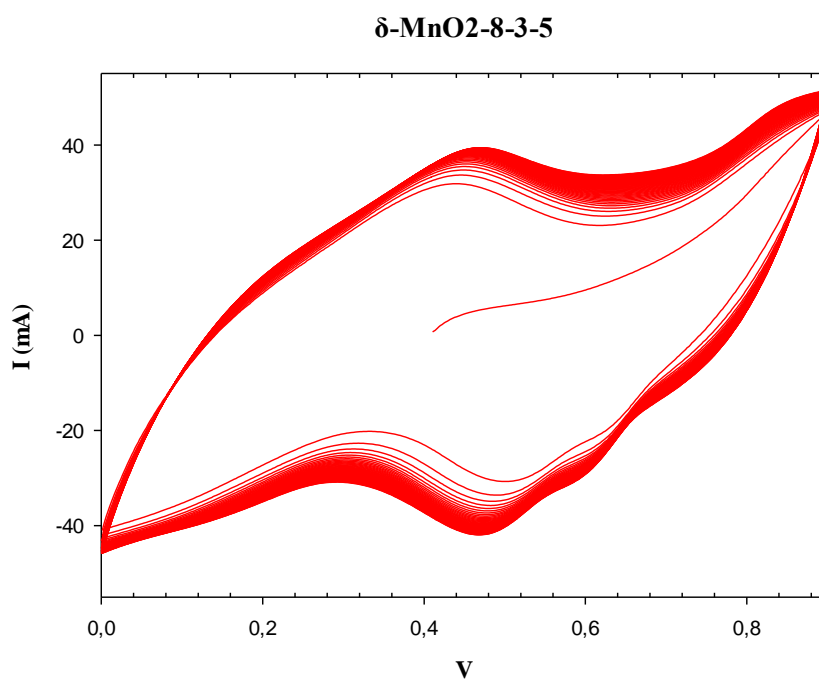
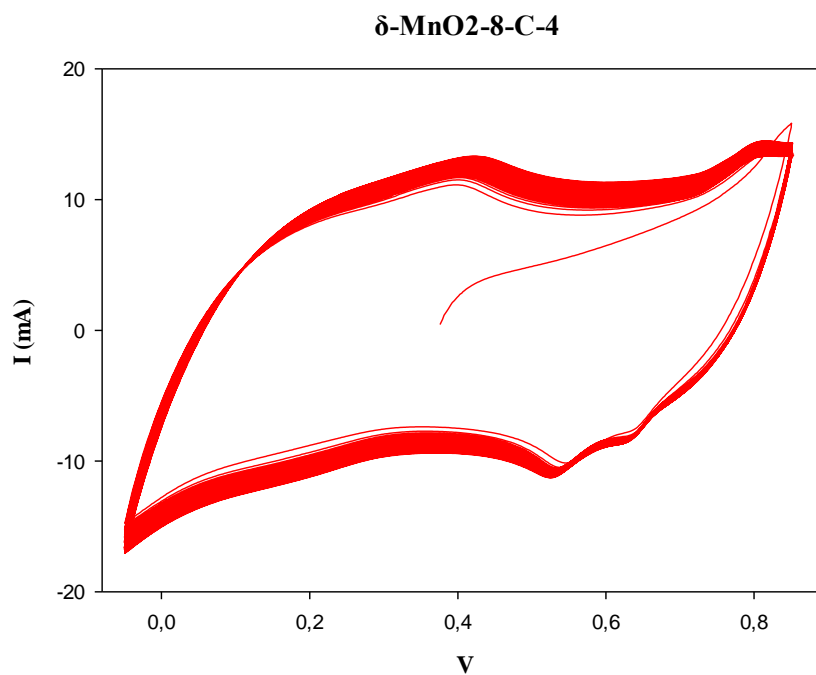


Figure 17 A cathodic and anodic peak can be observed at 0.47V and 0.45V, respectively, for  $\delta\text{-MnO}_2\text{-8-3-5}$ .



*Figure 18 A cathodic and anodic peak can be observed at 0.52V and 0.42V, respectively, for  $\delta$ -MnO<sub>2</sub>-8-C-4.*

## 5 Discussion

---

The goal of this thesis has been to investigate if carbon added during synthesis is better than carbon mixed in during processing. Two variations of carbon have been used, namely Ketjenblack (during synthesis), and Acetylene Black (during processing). In the following sections the results from materials characterization and electrochemical characterization are evaluated and discussed.

### 5.1 Materials characterization

#### 5.1.1 X-ray diffraction

XRD measurements were performed with D-8 Focus Diffractometer. All three materials seem to contain Birnessite, Hausmannite, and Feitknechtite. Feitknechtite is the most uncertain of the three elements, as Birnessite is the intended material and Hausmannite may form during synthesis and drying. Ghodbane et al.(3) found the following Birnessite peaks:  $2\theta=12.2, 24.7, 36.9, 65.7$ . As seen in on Table 4, these values are similar to  $\delta\text{-MnO}_2\text{-8-F-2}$ , with  $2\theta=12.2, 24.8, 37.1, 62.9$ . The last peak is shifted slightly to the left compared to Ghodbane.

In order to compare the materials,  $\delta\text{-MnO}_2\text{-8-F-2}$  is considered as the baseline material. If we look at  $\delta\text{-MnO}_2\text{-8-3}$ , the first three peaks (1,2,3) are slightly shifted to the right. However, during the last three peaks there are dissimilarities, indicating slight variations in the powder. Figure 8 confirms that some peaks are missing on  $\delta\text{-MnO}_2\text{-8-F-2}$  compared to the other two powders.  $\delta\text{-MnO}_2\text{-8-C}$  contains Ketjenblack, and it was expected to find carbon in some of the peaks. However, most of the peaks can be identified similarly to  $\delta\text{-MnO}_2\text{-8-3}$  and  $\delta\text{-MnO}_2\text{-8-F-2}$ . (see Figure 5 and 6). Peak 1 is shifted to the right compared to  $\delta\text{-MnO}_2\text{-8-F-2}$ . but is very similar to  $\delta\text{-MnO}_2\text{-8-3}$ .

In conclusion, all powders have Birnessite. Slight variations in d-spacing indicate that there is different amounts of intercalated atoms in the respective materials. This is probably caused by slight variations of synthesis parameters. However, the XRD measurements are highly dependent on how accurate the samples are prepared prior to testing. Human error might have affected the obtained d-spacings and results. It is also observed that no carbon has been identified  $\delta\text{-MnO}_2\text{-8-C}$ . This is probably an error, and some of the smaller peaks may have been dismissed during characterization.

### 5.1.2 Nitrogen adsorption experiments

Surface measurements were taken using a BET 5-point fingerprint technique. Surface areas of  $\delta$ -MnO<sub>2</sub>-8-F-2,  $\delta$ -MnO<sub>2</sub>-8-3,  $\delta$ -MnO<sub>2</sub>-8-F-C were measured to 46 m<sup>2</sup>/g, 66<sup>2</sup>/g, 408 m<sup>2</sup>/g, respectively. Their pore sizes were 2.08 nm, 21.33 nm, 2.07 nm, respectively.  $\delta$ -MnO<sub>2</sub>-8-F-2 and  $\delta$ -MnO<sub>2</sub>-8-F-C had almost identical pore sizes.  $\delta$ -MnO<sub>2</sub>-8-3 had much larger pores, by a factor of 10. This may have influenced the capacitance of the materials, which will be discussed during chapter 5.2 - Electrochemical characterization".

Similar synthesis parameters were used for all three powders, except  $\delta$ -MnO<sub>2</sub>-8-F-C which had Ketjenblack mixed in during initial stages, and  $\delta$ -MnO<sub>2</sub>-8-3 was titrated instead of poured. The Ketjenblack's measured surface area was 1435 m<sup>2</sup>/g. This explains the high surface area of  $\delta$ -MnO<sub>2</sub>-8-F-C. The accuracy of these tests is to some degree uncertain, because BET is influenced by external and internal factors. Variations in temperature, pressure, and the size of the adsorbed gas could influence the obtained results. It is also possible that the test tubes had small amounts of foreign elements in them. cleaned.(27, 28)

### 5.1.3 Thermogravimetric analysis

During mixing, a lot of carbon got stuck to the sides of the beakers (didn't mix with the MnO<sub>2</sub> mud). This means that the carbon put in, was not the same as the carbon that ended up in the powder. TGA was used to measure the carbon content of  $\delta$ -MnO<sub>2</sub>-8-F-C more accurately.

A small amount of powder (0.149mg) was tested. A background was performed to eliminate disturbance in the machine. Unfortunately, the background's initial temperature was 35°C, whereas the initial temperature of the analysis was 25°C. The difference in temperature might have been a contributing factor in the first peak in Figure 9. This peak is thought to be the result of buoyancy, which is caused by temperature and rate of change.(29) The first mass loss occurred at ~100 °C, which can be attributed to the phase change of water. As seen in Figure 9, the next loss of mass occurred between 93.1-68.1 wt%, yielding 25%wt loss. This is likely due to the phase change of carbon (the carbon got burnt of).

The accuracy of these measurements could have been improved by using a more inert atmosphere such as argon. Having equal starting temperature would likely have eliminated some of the buoyancy peak. This peak could also likely have been eliminated by using a newer TGA, as they are more effective at removing such disturbances from the measurements. The

measured carbon content was done mainly by hand. Having some way to automatically measure this would also likely have improved the results.

## 5.2 Electrochemical characterization

### 5.2.1 Constant current

Table 6 show the difference in capacitance between short and long cycles, Ketjenblack and Acetylene black based electrodes, and the current stages.  $\delta\text{-MnO}_2\text{-8-3-(1,5)}$  are both short cycled electrodes.  $\delta\text{-MnO}_2\text{-8-3-1}$  starts about 26 F/g higher on the 2<sup>th</sup> cycle than  $\delta\text{-MnO}_2\text{-8-3-5}$ , and ends about 24 F/g higher on the 9<sup>th</sup> cycle. The trend keeps going on all currents, where  $\delta\text{-MnO}_2\text{-8-3-1}$  is 13, 14, 14, 25 F/g higher at 0.2, 0.5, 1.0, 2.0 A/g respectively (9<sup>th</sup> cycle). This indicates that the electrodes are similar. The variations here could be caused by the way the electrodes were made. The paste was applied manually by hand, and some regions were naturally thicker than others. Unfortunately, time only allowed for two short cycles on these electrodes.

Standard deviation for the Ketjenblack based electrodes was calculated to be  $455 \pm 32$  F/g on 0.1 A/g. This value is reasonable compared to the Acetylene Black based electrodes. However, for the remaining currents the following standard deviations were observed:  $376 \pm 74$  F/g on 0.2 A/g,  $330 \pm 67$  F/g on 0.5 A/g,  $292 \pm 70$  F/g on 1.0 A/g,  $244 \pm 88$  F/g on 2.0 A/g. There is a relatively large variation between the electrodes. For example, the last measurement (2.0 A/g) of  $\delta\text{-MnO}_2\text{-8-C-3}$  only had 138 F/g at the 9<sup>th</sup> cycle. The same electrode had a very good capacitance at 0.1 A/g, at 440 F/g at 9<sup>th</sup> cycle. That's a 74 % capacitance loss during 40 cycles on different currents. The electrode had high stability during each stage, meaning the capacitance fluctuated little during each stage. During testing, mass loss was observed in the cell for  $\delta\text{-MnO}_2\text{-8-C-3}$ . (powder was observed floating in the cell), which could account for the loss of capacitance during the last 10 cycles. In general, there was little evidence of loss of mass from the electrodes.

The highest capacitance was recorded from the Ketjenblack electrode  $\delta\text{-MnO}_2\text{-8-C-4}$ , at the 9<sup>th</sup> cycle, 0.1 A/g. It reached the high capacitance of 501 F/g during discharge. All Ketjenblack electrodes had higher capacitance during the first 9 cycles, than the Acetylene Black based electrodes. With the exception being 1.0 A/g for  $\text{MnO}_2\text{-8-3-(1,5)}$ , were the Acetylene Black electrodes had higher capacitance than  $\delta\text{-MnO}_2\text{-8-C-(3,4)}$ . In general, the Ketjenblack based electrodes performed better during most stages, when it comes to capacitance. However, the

Acetylene Black electrodes seemed to be more stable. They also seemed to activate less than the Ketjenblack electrodes, indicating a smaller change in structure during cycle. The rate capability of the electrodes was calculated, and listed in Table 6. The best performing Ketjenblack electrodes with regard to high capacitance ( $\delta$ -MnO<sub>2</sub>-8-C-(4,6)) had the highest rate capability as well (of the Ketjenblack based electrodes). No mass loss was observed during  $\delta$ -MnO<sub>2</sub>-8-3-(1,5), and they both had rate capabilities at 69-71%. Some mass loss was observed at  $\delta$ -MnO<sub>2</sub>-8-2-F (which is fair, since the electrode was cycled for nearly three weeks). A parallel may then be drawn to how well the electrodes were made, and their rate capability.

The author recognizes that the use of Acetylene Black vs Ketjenblack may be causing the difference in capacitance. The fact that these powders are two different variations of carbon black might influence the results a fair bit. These results may also be an indication that mixing carbon directly into the MnO<sub>2</sub> during synthesis might be beneficial. Another possibility may be that Ketjenblack increase capacitance more than Acetylene Black. Or it might just be the increased carbon content (25% vs 15%) The stability of the electrodes could probably have been increased by improving the processing part. The high surface area made it difficult to find the right ratio of solvent vs powder. This made the electrodes quite dry when applied to the electrode substrate. This may account for mass loss during testing. The Ketjenblack based electrodes had ~2% more binder than the Acetylene Black electrodes (16% vs 14%). This should have led to less conductivity in the Ketjenblack based electrodes. Being able to fine tune this, could in turn also increase the capacitance quite a bit, as these are both high amounts of binder. It should also be noted that when a higher amount of carbon is added, more EDLC charging could take place, which may account for the added capacitance.

This study has been inspired by Ghodbane et al's(3) work, as mentioned during the introduction. While there are slight variations, the setup is similar. During cycling Ghodbane's team achieved 225 F/g in 0.5 M K<sub>2</sub>SO<sub>4</sub> for their Birnessite powder. They concluded that the bulk material is more important than the specific surface area of their electrodes.(3) This is in agreement with the fact that a higher capacitance is achieved at 0.1 A/g, were wetting of the bulk material is more likely. During their study they used CV to measure capacitance, whereas we used CC. We also used a 1 M MgSO<sub>4</sub> electrolyte. During this study higher capacitance values were achieved on all but one electrode, during all cycles. The measurement technique might have influenced this. Also, the ratio of Ketjenblack/Acetylene Black is a contributing factor. Mg<sup>2+</sup>'s ability to enter pores seem to be better than K<sup>+</sup> and is supported by ionic radius data.(6)



The electrode  $\delta\text{-MnO}_2\text{-8-F-2}$  was cycled 979 times. Here 30 cycles were done at 0.1 A/g, 50 cycles at 0.2 A/g, 45 cycles at 0.5 A/g, and 854 cycles at 1.0 A/g. At the optimal 0.1 A/g, the capacitance increased from 440 to 474 F/g during the first 30 cycles. This is a 7.2% increase in capacitance, most likely caused by activation. During the other three stages the capacitance fell slightly. At 0.2 A/g it fell 1.5%, at 0.5 A/g it fell 2.9%, at 1.0 A/g it fell 22.9%. The total loss from the highest measured value 474 F/g, until the last cycle at 236 F/g, was 50.4%. Also, some material loss was observed after testing. During the test it was also an 8h period without nitrogen cycling through the cell. Sadly, the equipment was disconnected accidentally during testing, so the full test of 1175 cycles was not performed. Also, the surface area of this material was slightly lower than that of the  $\delta\text{-MnO}_2\text{-8-3}$  powder. Still, it had higher capacitance at every stage.  $\delta\text{-MnO}_2\text{-8-3}$  was made by titration for 1 hour 20 minutes, while the  $\delta\text{-MnO}_2\text{-8-F-2}$  powder was made by pouring for 35. Since  $\delta\text{-MnO}_2\text{-8-3}$  had much larger pores compared to  $\delta\text{-MnO}_2\text{-8-F-2}$  (2.08 nm vs 21.33 nm), it is likely that this influenced the total capacitance of the electrodes as well. This is caused by the increased energy requirements for ions to enter pores when the pores become smaller. Thus, more energy may be released during discharge.(2, 8, 9)

### 5.2.2 CV curves

Figure 16, 17, 18 all show distinct CV curves for the electrodes  $\delta\text{-MnO}_2\text{-8-F-2}$ ,  $\delta\text{-MnO}_2\text{-8-C-4}$  and  $\delta\text{-MnO}_2\text{-8-3-5}$ . During both reduction and oxidation, clear cathodic and anodic peaks are visible. For example:  $\delta\text{-MnO}_2\text{-8-F-2}$  had cathodic peak at 0.44V, and an anodic peak at 0.48V. At this point the reaction is diffusion limited. Ghodbane et al.(17) found similar CV curves during cycling. They also investigated the curves with XRD during cycling. They observed a reversible intercalation/deintercalation process of cations while cycling. The materials used during this thesis is similar to the ones used Ghodbanes study. Which gives an indication that similar reactions take place as the given peaks.

## 6 Conclusion

---

In this study,  $\delta$ -MnO<sub>2</sub> composite electrodes were tested. It was attempted to figure out if Ketjenblack; added during synthesis or Acetylene Black; added during processing, would yield the better electrodes. Loosely translated, better means higher capacitance and stability. XRD, BET and TG was used to characterize the materials. The electrode was wetted for 6 hours, and then cyclic voltammetry was used to activate the electrode. Constant current was used to electrochemically cycle the material.

During XRD similar peaks were identified on all the materials. Some variations in d-spacing was observed, and some Birnessite peaks were missing in  $\delta$ -MnO<sub>2</sub>-8-C. Also, all powders seemed to have Birnessite, Feitknechtite and Hausmannite. All powders had characteristic Birnessite peaks  $2\theta = 12.2-12.5, 24.8-25, 37.0-37.1, 62.9-64.6$ . The BET specific surface areas of the powders were 46 m<sup>2</sup>/g, 66<sup>2</sup>/g, 408 m<sup>2</sup>/g, for  $\delta$ -MnO<sub>2</sub>-8-F-2,  $\delta$ -MnO<sub>2</sub>-8-3, and  $\delta$ -MnO<sub>2</sub>-8-F-C, respectively. However, when measuring pore size, it was noted that  $\delta$ -MnO<sub>2</sub>-8-3 had pore sizes in the mesopore region at ~21 nm, while the other two powders mainly had micropores around 2 nm. The powders with the smallest pores, also had the highest capacitance (as long as the ion fits), which is supported by the literature.

High values of 501 F/g for  $\delta$ -MnO<sub>2</sub>-8-C, 474 F/g for  $\delta$ -MnO<sub>2</sub>-8-F-2, and 447 F/g for  $\delta$ -MnO<sub>2</sub>-8-3 was measured during the 9<sup>th</sup> cycle at 0.1 A/g. The measured capacitance was still climbing at the end of the first 10 cycles, indicating further activation of the materials. These capacitance values are unusually high for Birnessite MnO<sub>2</sub>. Literature normally report capacitance values around 100-200 F/g. The Ketjenblack based electrodes had the highest capacitance values overall, which is a indication that adding Ketjenblack during synthesis will improve supercapacitor electrodes. However, too few parallels have been tested, and more research is needed.

## 7 Future works

---

- ❖ Several long cycles could be performed on the various powders to investigate the cycling stability and reproducibility over time.
- ❖ Several electrolytes could be tested so that results could be compared in different environments. examples of these could be  $\text{Na}_2\text{SO}_4$ ,  $\text{K}_2\text{SO}_4$ , Li...., etc.
- ❖ Several retests on XRD, BET, TG could be done, to see if the results persist.
- ❖ The binder/ $\text{MnO}_2$  ratio could be adjusted to see if +the capacitance increased or declined. The binders conductivity could also be improved as Dong et al did during their study. (7)
- ❖ The effect of  $\delta\text{-MnO}_2$  formation in titration vs pouring.
- ❖ The effect of  $\delta\text{-MnO}_2$  formation when adding carbon to the mix during synthesis.

## 8 References

---

1. Dubal DP, Wu YP, Holze R. Supercapacitors: from the Leyden jar to electric busses. *ChemTexts*. 2016;2(3):13.
2. Lu M, Beguin F, Frackowiak E. Supercapacitors : Materials, Systems and Applications. Weinheim, GERMANY: John Wiley & Sons, Incorporated; 2013.
3. Ghodbane O, Pascal J-L, Favier F. Microstructural effects on charge-storage properties in MnO<sub>2</sub> -based electrochemical supercapacitors. *ACS Applied Materials and Interfaces*. 2009;1(5):1130-9.
4. Bagotskiĭ VS, Skundin AM, Volkovich YM. Electrochemical power sources : batteries, fuel cells, and supercapacitors: John Wiley & Sons; 2015.
5. Wang H, Yoshio M. Effect of water contamination in the organic electrolyte on the performance of activated carbon/graphite capacitors. *Journal of Power Sources*. 2010;195(1):389-92.
6. Greenwood NN, Earnshaw A. 5.3.1 Introduction. 2nd Edition ed: Elsevier; 1997. 1-2 p.
7. Dong J, Wang Z, Kang X. The synthesis of graphene/PVDF composite binder and its application in high performance MnO<sub>2</sub> supercapacitors. *Colloids and Surfaces A: Physicochemical and Engineering Aspects*. 2016;489:282-8.
8. Yu AaVC, JiuJun Zhang. Electrochemical supercapacitors for energy storage and delivery; fundamentals and applications. Portland: CRC Press; 2013. p. 356
9. Feng G, Qiao R, Huang J, Sumpter B, Meunier V. Atomistic Insight on the Charging Energetics in Subnanometer Pore Supercapacitors. *J Phys Chem C*. 2010;114(41):18012-6.
10. Ding Y, Zhang Z. Nanoporous metals for advanced energy technologies: Springer; 2016.
11. Aylward GH, Findlay TJV. Si chemical data. 6th ed. ed. Milton: Wiley; 2008.
12. Salanne M, Rotenberg B, Naoi K, Kaneko K, Taberna PL, Grey CP, et al. Efficient storage mechanisms for building better supercapacitors. 2016. p. 16070.
13. Xu C, Shi S. Manganese dioxide based supercapacitors2014. 85-132 p.
14. Albering JH. Structural Chemistry of Manganese Dioxide and Related Compounds2011. 87-123 p.
15. Feng Q, Kanoh H, Ooi K. Manganese oxide porous crystals1999. 319-33 p.
16. Brousse T, Toupin M, Dugas R, Athouël L, Crosnier O, Bélanger D. Crystalline MnO<sub>2</sub> as possible alternatives to amorphous compounds in electrochemical supercapacitors. *Journal of the Electrochemical Society*. 2006;153(12):A2171-A80.
17. Ghodbane O, Ataherian F, Wu NL, Favier F. In situ crystallographic investigations of charge storage mechanisms in MnO<sub>2</sub> -based electrochemical capacitors. *Journal of Power Sources*. 2012;206:454-62.
18. Zhang X, Liu X, Li B, Chu Q, Wang Y, Zhao X, et al. Rapid microwave synthesis of [delta]-MnO<sub>2</sub> microspheres and their electrochemical property. *Journal of Materials Science Materials in Electronics*. 2013;24(7):2189-96.

19. Cao LL, Yu BZ, Cheng T, Zheng XL, Li XH, Li WL, et al. Optimized K<sup>+</sup> pre-intercalation in layered manganese dioxide nanoflake arrays with high intercalation pseudocapacitance. *Ceramics International*. 2017;43(17):14897-904.
20. Qi J-Q, Guo R, Zhao F-f, Li W-Y, Yao W-Q. Tailoring the lattice structure of manganese oxides under electric field and improving the supercapacity of them. *Lausanne*:2017. p. 134-9.
21. Cullity BD. *Elements of X-ray diffraction*. 2nd ed. ed. Reading, Mass: Addison-Wesley; 1978.
22. Pecharsky VK, Zavalij PY. *Fundamentals of powder diffraction and structural characterization of materials*2005. 1-741 p.
23. Mansfield M, O'Sullivan C. *Understanding physics*. 2nd ed. ed. Chichester: Wiley; 2011.
24. Jenkins R, Snyder RL. *Introduction to X-ray powder diffractometry*. New York: Wiley; 1996.
25. Sing KSW, Rouquerol F, Rouquerol J. 5 - Classical Interpretation of Physisorption Isotherms at the Gas-Solid Interface. *Adsorption by Powders and Porous Solids (Second Edition)*. Oxford: Academic Press; 2014. p. 159-89.
26. Naderi M. Chapter Fourteen - Surface Area: Brunauer-Emmett-Teller (BET) A2 - Tarleton, Steve. *Progress in Filtration and Separation*. Oxford: Academic Press; 2015. p. 585-608.
27. Ismail IMK. Cross-sectional areas of adsorbed nitrogen, argon, krypton, and oxygen on carbons and fumed silicas at liquid nitrogen temperature. *Langmuir*. 1992;8(2):360-5.
28. Hanaor DAH, Ghadiri M, Chrzanowski W, Gan Y. Scalable Surface Area Characterization by Electrokinetic Analysis of Complex Anion Adsorption. *Langmuir*. 2014;30(50):15143-52.
29. Prime RB, Bair HE, Vyazovkin S, Gallagher PK, Riga A. *Thermogravimetric Analysis (TGA). Thermal Analysis of Polymers: John Wiley & Sons, Inc.*; 2008. p. 241-317.
30. Qu D, Shi H. Studies of activated carbons used in double-layer capacitors. *J Power Sources*. 1998;74(1):99-107.
31. Oldham KB, Myland JC, Bond AM. *Electrochemical Science and Technology: Fundamentals and Applications*. Chichester, UK: Chichester, UK: John Wiley & Sons, Ltd; 2011.
32. Bard AJ, Faulkner LR. *Electrochemical methods : fundamentals and applications*. 2nd ed. ed. New York: Wiley; 2001.
33. Elgrishi N, Rountree KJ, McCarthy BD, Rountree ES, Eisenhart TT, Dempsey JL. A Practical Beginner's Guide to Cyclic Voltammetry. *Journal of Chemical Education*. 2018;95(2):197-206.
34. Flexcell - Test cells for gas diffusion electrodes: Gaskatel; [Instruction manual + basic information about 3-cell used during testing.]. Available from: [http://www.gaskatel.de/eng/produkte/flexcell/eng\\_flexcell\\_index.html](http://www.gaskatel.de/eng/produkte/flexcell/eng_flexcell_index.html).

## Appendice I Electrochemical cycling – Constant current

$\delta$ -MnO<sub>2</sub>-8-F-2

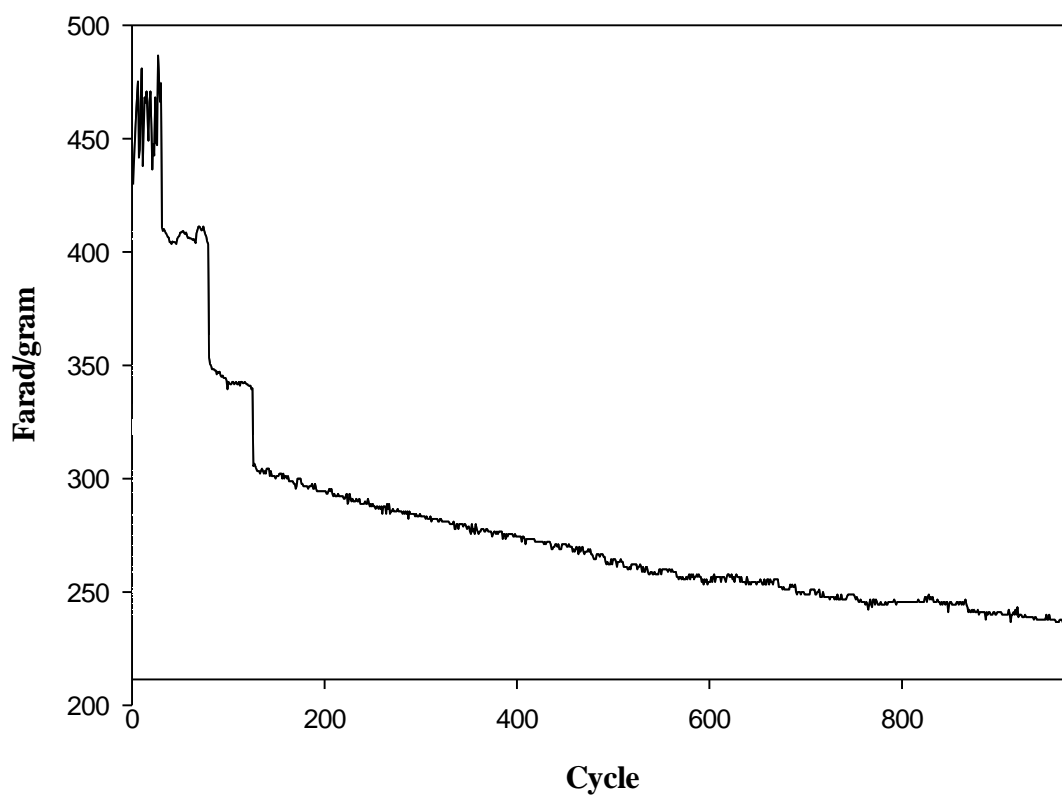


Figure 19 Complete CC of  $\delta$ -MnO<sub>2</sub>-8-F-2 to illustrate change in capacitance over different values.

Below are the remaining discharge curves for all the short constant current curves.

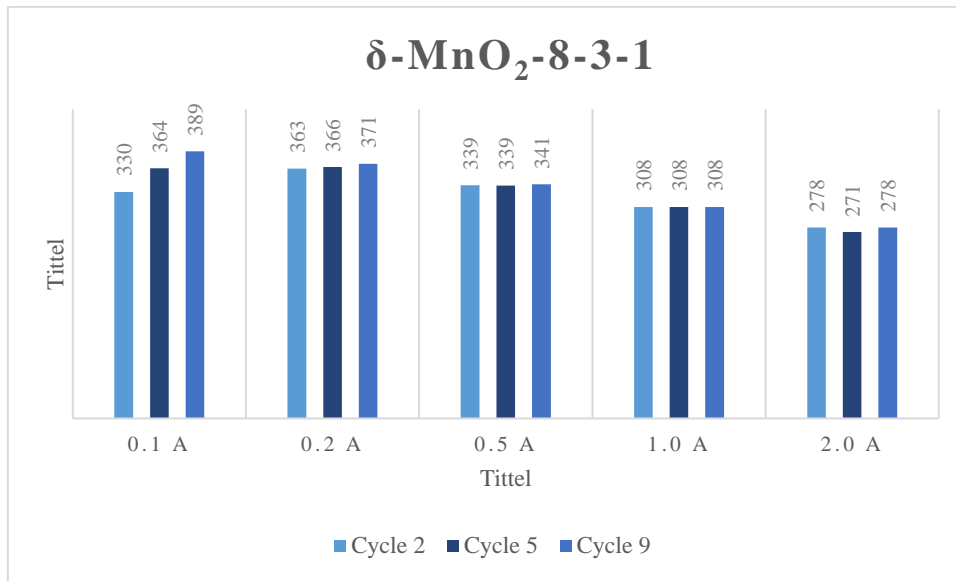


Figure 20 Constant current discharge capacitance values achieved at 2, 5, 9 cycles on 0.1, 0.2, 0.5, 1.0, 2.0 A/g for  $\delta\text{-MnO}_2\text{-8-3-1}$

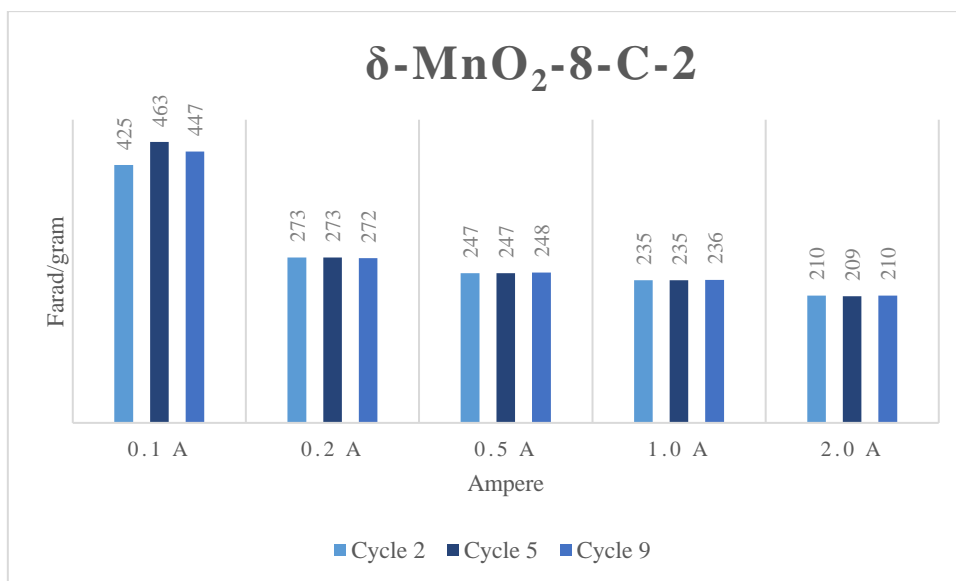


Figure 21 Constant current discharge capacitance values achieved at 2, 5, 9 cycles on 0.1, 0.2, 0.5, 1.0, 2.0 A/g for  $\delta\text{-MnO}_2\text{-8-C-2}$

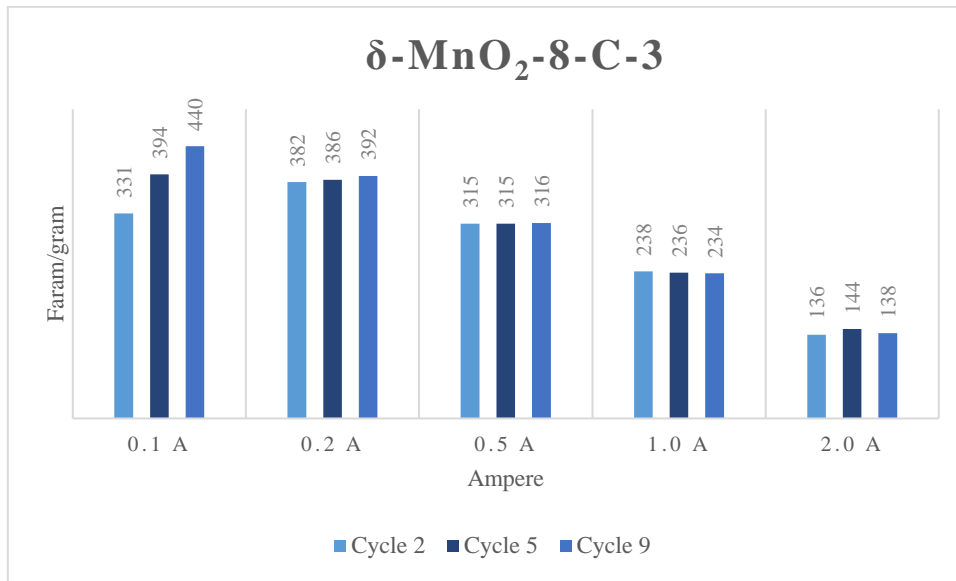


Figure 22 Constant current discharge capacitance values achieved at 2, 5, 9 cycles on 0.1, 0.2, 0.5, 1.0, 2.0 A/g for  $\delta\text{-MnO}_2\text{-8-C-3}$

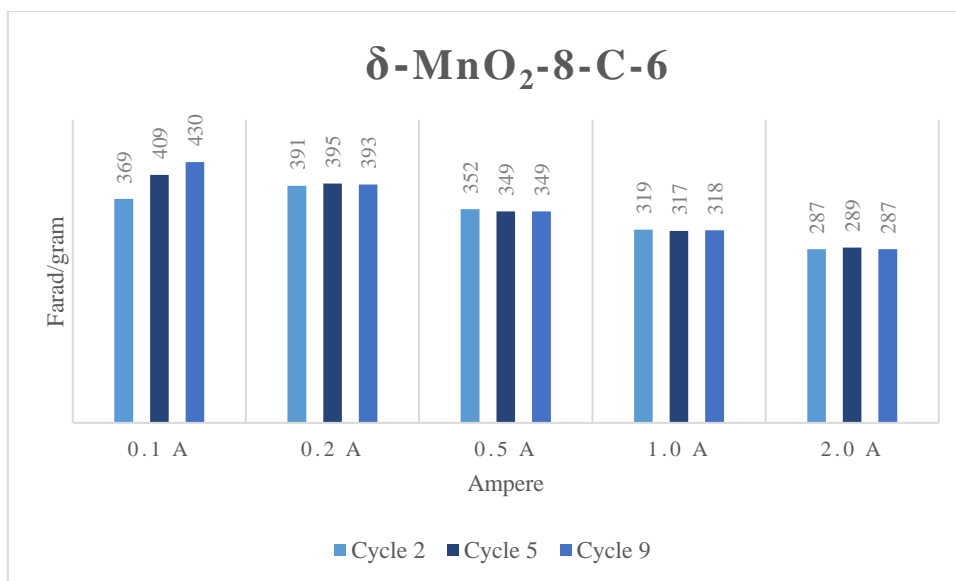


Figure 23 Constant current discharge capacitance values achieved at 2, 5, 9 cycles on 0.1, 0.2, 0.5, 1.0, 2.0 A/g for  $\delta\text{-MnO}_2\text{-8-C-6}$



## Appendice II Electrochemical cycling Current Voltage

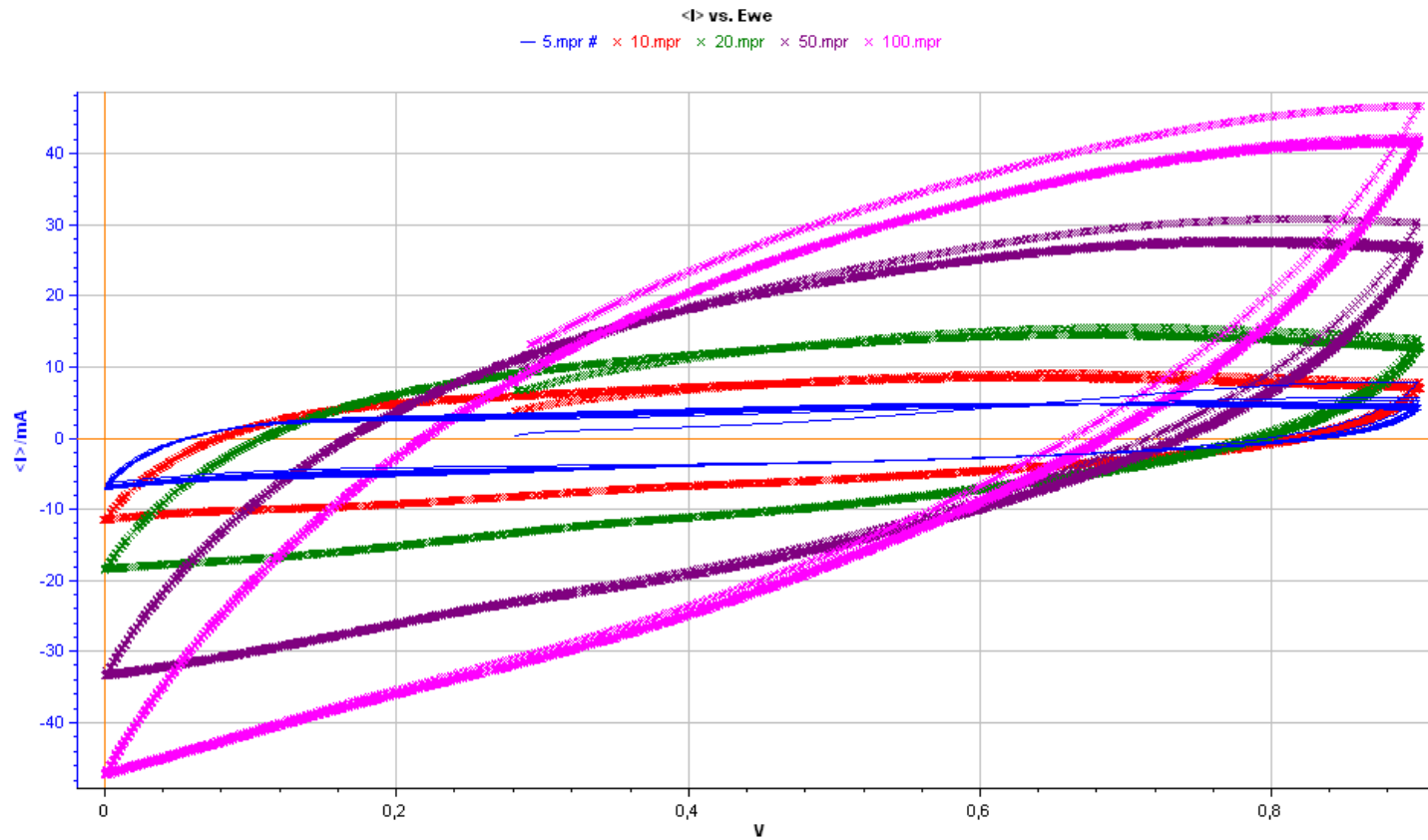


Figure 24 CV 5-10-20-50-100 mv/s test after long cycle to check for stability of the electrode Figure 25 CV 5-10-20-50-100 mv/s test after long cycle to check for stability of the electrode.

## Appendice III Parameters used during synthesis

Table 7 Complete list of parameters used during synthesis.

Powders	$\delta$ -MnO <sub>2</sub> -8-F-2	$\delta$ -MnO <sub>2</sub> -8-3	$\delta$ -MnO <sub>2</sub> -8-C
MnO <sub>4</sub> <sup>-</sup> /Mn <sup>2+</sup> -ratio	0.36	0.36	0.36
Beaker	MnO <sub>4</sub> <sup>-</sup> , OH <sup>-</sup>	MnO <sub>4</sub> <sup>-</sup> , OH <sup>-</sup>	MnO <sub>4</sub> <sup>-</sup> , OH <sup>-</sup> , Carbon*
Burette/beaker	Mn <sup>2+</sup>	Mn <sup>2+</sup>	Mn <sup>2+</sup>
Concentration, MnO <sub>4</sub> <sup>-</sup> [M] prior to mixing	0.1	0.1	0.1
Concentration, Mn <sup>2+</sup> [M] prior to mixing	0.28	0.28	0.28
Volume after mixing	0.4L	0.4L	0.4L
pH before mixing MnO <sub>4</sub> <sup>-</sup> og Mn <sup>2+</sup> (ca.)	14+	14+	14+
Temperature beaker when mixing [°C]	3	1	4-6°C
Temperature burette when mixing [°C]	2	1	3
Temperature beaker after mixing [°C]	3	2	6
Titration speed [mL/s]	Poured over 35 sec.	1t, 20min	Poured over 20 sec
Mixing speed [1/min]	7	7	7
Agingtemperature [°C]	ice, no mixing	ice, no mixing	ice, no mixing
Agingtime [days]	1	1	1
pH before cleaning	14+	14+	14+
Dryingtemperature[°C]	60°C	60°C	60°C
Time spent drying [hours]	20	18t 30 min	19
BET [m <sup>2</sup> /g], 3Flex(12 hours degas)	53,578	55	408,46

## Appendice IV BET Ketjenblack values

### Summary Report

#### Surface Area

Single point surface area at  $p/p^0 = 0.198441800$ : 1387.5124 m<sup>2</sup>/g

BET Surface Area: 1435.2096 m<sup>2</sup>/g

Langmuir Surface Area: 1968.8284 m<sup>2</sup>/g

t-Plot Micropore Area: 42.2850 m<sup>2</sup>/g

t-Plot External Surface Area: 1392.9246 m<sup>2</sup>/g

BJH Adsorption cumulative surface area of pores  
between 17.000 Å and 3000.000 Å diameter: 1484.6609 m<sup>2</sup>/g

BJH Desorption cumulative surface area of pores  
between 17.000 Å and 3000.000 Å diameter: 1577.7833 m<sup>2</sup>/g

#### Pore Volume

Single point adsorption total pore volume of pores  
less than 898.583 Å diameter at  $p/p^0 = 0.977970369$ : 2.622709 cm<sup>3</sup>/g

Single point desorption total pore volume of pores  
less than 1249.153 Å diameter at  $p/p^0 = 0.984256051$ : 3.663073 cm<sup>3</sup>/g

t-Plot micropore volume: 0.007980 cm<sup>3</sup>/g

BJH Adsorption cumulative volume of pores  
between 17.000 Å and 3000.000 Å diameter: 3.200497 cm<sup>3</sup>/g

BJH Desorption cumulative volume of pores  
between 17.000 Å and 3000.000 Å diameter: 3.773614 cm<sup>3</sup>/g

#### Pore Size

Adsorption average pore width (4V/A by BET): 73.0962 Å

Desorption average pore width (4V/A by BET): 102.0916 Å

BJH Adsorption average pore diameter (4V/A): 86.228 Å

BJH Desorption average pore diameter (4V/A): 95.669 Å

Figure 26 BET test of the Ketjenblack used in this thesis, by courtesy of SINTEF.

## Appendix V BET Powders

### Summary Report

#### Surface Area

Single point surface area at P/Po = 0,300000000: 44,1177 m<sup>2</sup>/g

BET Surface Area: 45,8600 m<sup>2</sup>/g

Langmuir Surface Area: 70,5171 m<sup>2</sup>/g

t-Plot Micropore Area: 2,3473 m<sup>2</sup>/g

t-Plot external surface area: 43,5127 m<sup>2</sup>/g

BJH Adsorption cumulative surface area of pores  
between 17,000 Å and 3 000,000 Å diameter: 23.903 m<sup>2</sup>/g

D-H Adsorption cumulative surface area of pores  
between 17,000 Å and 3 000,000 Å diameter: 22.062 m<sup>2</sup>/g

#### Pore Volume

t-Plot micropore volume: 0,000775 cm<sup>3</sup>/g

BJH Adsorption cumulative volume of pores  
between 17,000 Å and 3 000,000 Å diameter: 0,012356 cm<sup>3</sup>/g

#### Pore Size

BJH Adsorption average pore diameter (4V/A): 20,676 Å

D-H Adsorption average pore diameter (4V/A): 20,926 Å

*Figure 27 BET report for d-MnO<sub>2</sub>-8-F-2*

## Summary Report

### Surface Area

Single point surface area at  $P/P_0 = 0,300000000$ : 64,0023 m<sup>2</sup>/g

BET Surface Area: 66,1305 m<sup>2</sup>/g

Langmuir Surface Area: 858,6083 m<sup>2</sup>/g

t-Plot external surface area: 68,2048 m<sup>2</sup>/g

BJH Adsorption cumulative surface area of pores  
between 17,000 Å and 3 000,000 Å diameter: 64.010 m<sup>2</sup>/g

BJH Desorption cumulative surface area of pores  
between 17,000 Å and 3 000,000 Å diameter: 65,8574 m<sup>2</sup>/g

D-H Adsorption cumulative surface area of pores  
between 17,000 Å and 3 000,000 Å diameter: 62.795 m<sup>2</sup>/g

D-H Desorption cumulative surface area of pores  
between 17,000 Å and 3 000,000 Å diameter: 64,3467 m<sup>2</sup>/g

### Pore Volume

Single point adsorption total pore volume of pores  
less than 403,122 Å diameter at  $P/P_0 = 0,950000000$ : 0,161243 cm<sup>3</sup>/g

Single point desorption total pore volume of pores  
less than 403,122 Å diameter at  $P/P_0 = 0,950000000$ : 0,211207 cm<sup>3</sup>/g

t-Plot micropore volume: -0,001465 cm<sup>3</sup>/g

BJH Adsorption cumulative volume of pores  
between 17,000 Å and 3 000,000 Å diameter: 0,337353 cm<sup>3</sup>/g

BJH Desorption cumulative volume of pores  
between 17,000 Å and 3 000,000 Å diameter: 0,338361 cm<sup>3</sup>/g

### Pore Size

Adsorption average pore diameter (4V/A by BET): 97,5305 Å

Desorption average pore diameter (4V/A by BET): 127,7519 Å

---

*Figure 28 BET report for d-Mn02-8-3*

## Summary Report

### Surface Area

Single point surface area at  $P/P_0 = 0,300000000$ : 400,3573 m<sup>2</sup>/g

BET Surface Area: 408,4666 m<sup>2</sup>/g

Langmuir Surface Area: 638,9039 m<sup>2</sup>/g

t-Plot Micropore Area: 7,3729 m<sup>2</sup>/g

t-Plot external surface area: 401,0938 m<sup>2</sup>/g

BJH Adsorption cumulative surface area of pores  
between 17,000 Å and 3 000,000 Å diameter: 231.612 m<sup>2</sup>/g

D-H Adsorption cumulative surface area of pores  
between 17,000 Å and 3 000,000 Å diameter: 213.106 m<sup>2</sup>/g

### Pore Volume

t-Plot micropore volume: 0,002279 cm<sup>3</sup>/g

BJH Adsorption cumulative volume of pores  
between 17,000 Å and 3 000,000 Å diameter: 0,119579 cm<sup>3</sup>/g

### Pore Size

BJH Adsorption average pore diameter (4V/A): 20,652 Å

D-H Adsorption average pore diameter (4V/A): 20,919 Å

*Figure 29 BET report for d-MnO<sub>2</sub>-8-C*

